Dalton Transactions

ROYAL SOCIETY OF CHEMISTRY

PAPER

View Article Online
View Journal | View Issue

Cite this: *Dalton Trans.*, 2025, **54**, 15206

Structure of highly concentrated aqueous electrolyte solutions of transition metal chlorides and bromides

Éva G. Bajnóczi, †[a] Kajsa G. V. Sigfridsson Clauss [b] and Ingmar Persson *[a]

The structures of the complexes dominating in highly concentrated and 1.0 mol dm^{-3} aqueous solutions of first-row transition metal chlorides and bromides have been studied using large angle X-ray scattering (LAXS) and/or EXAFS. Of these systems, only zinc(II) chloride and bromide form inner-sphere complexes in dilute aqueous solutions. No inner-sphere complexes corresponding to dilute aqueous perchlorate solutions and $[M(H_2O)_6](ClO_4)_2$ solids were formed in 1.0 mol dm^{-3} aqueous solutions of the cobalt(II), nickel(II) and copper(II) chloride and bromide systems, according to the superimposing EXAFS spectra of these samples. A *cis*-dibromo complex dominates in a highly concentrated aqueous manganese(II) bromide solution, as that found in the solid state. In highly concentrated solutions of cobalt(II) and nickel (II) chloride and bromide and copper(II) chloride, one inner-sphere complex is formed, while the remaining halide ions are in the second coordination shell. In an almost saturated copper(II) bromide solution (5.67 mol dm^{-3}), a polynuclear complex based on hydrated *cis*-$CuBr_2$ units is formed with a significantly different structure than that observed in the solid state, *trans*-$[CuBr_2(H_2O)_2]$. In a highly concentrated zinc chloride solution, 11.81 mol dm^{-3}, with less than two water molecules per $ZnCl_2$ formula unit, a $[Zn_2Cl_4]$ complex is formed, where the zinc ions are three-coordinated in a triangular fashion. In a 5.60 mol dm^{-3} zinc bromide solution, a dimeric $[Zn_2Br_4(H_2O)_2]$ complex is formed, where the coordination around the zinc ions is distorted tetrahedral. These structures are different from those precipitated from saturated aqueous zinc chloride and bromide solutions, $[Zn(H_2O)_6][ZnCl_4]$, $[(H_2O)_5Zn{-}Cl{-}ZnCl_3]$ or $[Cl_3ZnClZn(H_2O)_4ClZnCl]_n$ and $[Zn(H_2O)_6][Zn_2Br_6]$. An increased stability of high-symmetry complexes is observed in the solid state, while in aqueous solution, complexes with maximized hydration seem to be favored.

Received 1st August 2025,
Accepted 5th September 2025

DOI: 10.1039/d5dt01840d

rsc.li/dalton

Introduction

Concentrated aqueous solutions of first-row transition metal halides have a range of technical applications. Aqueous manganese(II) chloride solutions play a crucial role as a micronutrient, benefiting plant growth and enhancing crop productivity by addressing manganese deficiency in soils with neutral or slightly alkaline pH.[1] Such solutions are also used in the production of manganese-based batteries.[2] Cobalt(II) chloride is a common visual moisture indicator due to its distinct colour change from blue to pink when hydrated. An important industrial application of copper(II) chloride is as a co-catalyst together with palladium(II) chloride in the oxidation of alkenes to ketones.[3] Concentrated aqueous zinc(II) chloride solutions dissolve cellulose in two steps. The solution penetrates the cellulose interior, and then, the Zn^{2+} and Cl^- ions break the hydrogen bonds. The cellulose's intermolecular and intramolecular hydrogen bonding breakage promotes the dissolution of cellulose.[4,5] Due to the high density of concentrated aqueous zinc bromide solutions, they are used in oil and natural gas wells to displace drilling mud when transitioning from the drilling phase to the completion phase or in well workover operations.[6] The density of such solutions makes them useful in holding back flammable oil and gas particles in high-pressure wells. Concentrated aqueous zinc bromide solutions are used as electrolytes in zinc bromide batteries.[7] Such solutions are also used as windows in hot cells due to their high absorbance of X-ray and gamma radiation, and they do not darken on exposure.[8] This is because any radiation damage lasts less than a millisecond, and the shield undergoes self-repair.[8]

Metal ion-ligand complex formation is a competition between the hydration/solvation strength of the metal ion and

[a]*Department of Molecular Sciences, Swedish University of Agricultural Sciences, P.O. Box 7015, SE–750 07 Uppsala, Sweden. E-mail: ingmar.persson@slu.se; Tel: +46–722164969*
[b]*MAX IV Laboratory, Lund University, Fotongatan 2, SE–221 00 Lund, Sweden*
† Present address: Wigner Research Centre for Physics, Konkoly–Thege Miklós út 29-33, H-1121 Budapest, Hungary.

the ligand, and their ability to bind to each other. As the concentration of the dissolved salt increases, the concentration of the free ligand increases, thereby increasing the probability of complex formation. At the same time, the amount of water available for the hydration of the ions decreases with increasing concentration, and at high concentrations, there is a deficit in the amount of water required for the complete hydration of the ions. Divalent first-row transition metal ions are strongly hydrated,[9,10] with two well-defined hydration shells in an aqueous solution,[11] Table 1. Double difference IR (DDIR) studies have shown that the M–O bond is much stronger than the (O–)H···O hydrogen bond in bulk water, while the hydrogen bonds between the first and second hydration spheres and the hydration of the chloride and bromide ions are weaker than the internal hydrogen bonds in bulk water,[12] Table 1. This means that in dilute aqueous solutions of MCl_2 or MBr_2, where M = divalent transition metal ion, 30 water molecules per formula unit are engaged in hydration: 6 + 12 (first and second hydration shells) of the metal ion, and 6 of the halide ions (one hydration shell). For the Jahn–Teller distorted copper(II) ion, it seems unlikely that the weakly bound water molecules in the axial positions can form a second hydration sphere.[13,14] This situation continues until the n_{H_2O}/n_{MX_2} ratio reaches 30–40, corresponding to a concentration of approximately 1.35–1.75 mol dm^{-3}. From this concentration, there is a competition for water between the second hydration sphere of the metal ion, the halide ions and bulk water. One set of solutions investigated in this study, 1.0 mol dm^{-3}, represents solutions with fairly high concentration but with a sufficient amount of water for complete hydration. The other set consists of saturated solutions, which in most cases have a deficit of water for the first-shell hydration of the metal and halide ions, with an n_{H_2O}/n_{MX_2} ratio of less than 18. The latter is compared with the structures of solids precipitating from oversaturated aqueous solutions.

Manganese(II), cobalt(II), nickel(II), copper(II) and zinc(II) form weak complexes with halide ions in dilute aqueous solutions in the order $Zn^{2+} \geq Cu^{2+} > Mn^{2+} > Co^{2+} > Ni^{2+}$, and $Cl^- > Br^- > I^-$, but the reported stability constants are scattered and ionic medium and strength dependent, Table S1 (SI). All manganese(II) halide compounds precipitated from aqueous solutions bind to the halide ions in the first coordination sphere. *cis*- and *trans*-$[MnCl_2(H_2O)_4]$, *cis*-$[MnBr_2(H_2O)_4]$ and *trans*-$[MnI_2(H_2O)_4]$ complexes, as well as double chloro- and bromo-bridged dimers and polymers, are reported in the solid state, Table S2 (SI). A large angle X-ray scattering (LAXS) study on concentrated aqueous manganese(II) chloride and bromide solutions, 4.74 and 5.09 mol dm^{-3}, respectively, with mean coordination numbers of 1.21 and 1.50, reported mean Mn–O and Mn–Cl, and Mn–O and Mn–Br bond distances of 2.18 and 2.49 Å, and 2.18 and 2.62 Å, respectively.[15] Similar results were reported in an EXAFS study, and a second hydration shell at 4.4 Å was identified.[16]

cis- and *trans*-$[CoCl_2(H_2O)_4]$ and *trans*-$[CoBr_2(H_2O)_4]$ complexes are reported in the solid state, while the iodide compound has the composition $[Co(H_2O)_6]I_2$ (Table S3, SI). Early LAXS studies on *ca.* 3.0 mol dm^{-3} aqueous solutions of cobalt(II) chloride and bromide showed a fully dissociated salt with a mean Co–O bond distance of 2.1 Å, and no Co–Cl or Co–Br interactions could be detected.[17,18] A LAXS study on concentrated aqueous cobalt(II) chloride solutions showed that the cobalt content was equally divided as hydrated cobalt(II) ions and monochlorocobalt(II) complexes.[19] LAXS studies on concentrated aqueous solutions with $[Cl^-]/[Co^{2+}]$ ratios of 3.4 and 4.0 show that the monochlorocobalt(II) complex is the dominating species with Co–O and Co–Cl bond distances of 2.14 and 2.35 Å, respectively.[20,21] In 3.0 mol dm^{-3}, aqueous solutions of cobalt(II) chloride with added lithium chloride showed an inner-sphere chloride complex at $[Cl^-]/[Co^{2+}]$ ratios of 6 and 7.[22] 2.8 and 4.2 mol dm^{-3} aqueous cobalt(II) bromide solutions showed partial formation of a monochlorocobalt(II) complex, $[CoBr_n(H_2O)_{6-n}]^{(2-n)+}$, where n = 0.28 and 0.60, respectively.[23]

cis- and *trans*-$[NiCl_2(H_2O)_4]$ and –$[NiBr_2(H_2O)_4]$ complexes, as well as a double chloro-bridged dimer, are reported in the solid state, Table S4 (SI). The structure of the $[NiBr(H_2O)_5]^+$ complex has been reported in the solid state,[24] while for iodide, the dissociated complex crystallizes from aqueous solution, $[Ni(H_2O)_6]I_2$, Table S4 (SI). A large number of LAXS and neutron scattering studies on concentrated aqueous nickel(II) chloride solutions have been reported, showing complete dissociation with mean Ni–O bond distances of 2.06 Å.[25–27] LAXS studies on concentrated aqueous nickel(II) bromide solutions have reported the formation of fractions of a monobromonickel(II) complex with mean Ni–O and Ni–Br bond distances of 2.06 and 2.61 Å, respectively.[28–30]

All reported crystal structures containing hydrated copper(II) chloride and bromide complexes have *trans* configuration, including a polymeric complex with a single bromide bridge, Table S5 (SI). An early LAXS study on 3.18 and 4.35 mol dm^{-3} aqueous copper(II) chloride solutions reported the formation of hydrated polymeric chlorocopper(II) complexes with double chloride bridges with the proposed mean compositions $[Cu_3Cl_6(H_2O)_8]$ and $[Cu_5Cl_{10}(H_2O)_{12}]$, respectively, with mean Cu–O and Cu–Cl bond distances of 1.93 and 2.43 Å, respectively.[31] A similar concentrated aqueous copper(II) chloride solution with an excess of hydrochloric acid reported an average structure of $[Cu_4Cl_{10}(H_2O)_8]^{2-}$ with mean Cu–O, Cu–Cl_{eq} and Cu–Cl_{ax} bond distances of 1.95, 2.27 and 2.6 Å,

Table 1 Hydration enthalpy (kJ mol^{-1}), hydration number, and O–D stretching frequency of the hydrating water molecules in water with 8% HDO

	ΔH°_{hydr} [a]	Hydration number[b]	ν(O–D)[c] (cm^{-1})
Mn^{2+}	−1841	6 + 12	2420
Co^{2+}	−1996	6 + 12	2428
Ni^{2+}	−2105	6 + 12	2418 + 2530
Cu^{2+}	−2100	6 + 8	2400 + 2530
Zn^{2+}	−2046	6 + 12	2418
Cl^-	−381	6	2530
Br^-	−347	6	2550

[a] Ref. 9. [b] Ref. 11. [c] Ref. 12.

respectively.[32] The structures of these polymeric structures in aqueous solution have large similarities with the crystal structure of copper(II) chloride dihydrate, Table S5 (SI). A LAXS study of a 3.0 mol dm^{-3} aqueous copper(II) chloride solution reported a mean coordination number of chloride of 1.2, with a mean Cu–Cl bond distance of 2.25 Å, 2.8 water oxygens at 1.954 Å, and two axial water molecules at 2.63 Å.[33] The structures of concentrated aqueous copper(II) bromide solutions were determined by LAXS in a concentration range of 1.016–4.364 mol dm^{-3}.[34] Similar structures were observed in the studied concentration range with two water molecules and two bromide ions in the equatorial plane and water molecules in the axial positions with mean Cu–O_{eq}, Cu–Br_{eq} and Cu–O_{ax} bond distances of 1.97, 2.44 and 2.45 Å, respectively. The mean coordination number of Br^- ions in the first coordination shell of copper(II) increased from 0.33 to 1.31 as the concentration of $CuBr_2$ increased from 1.016 to 4.364 mol dm^{-3}.

Precipitation from saturated aqueous zinc(II) chloride solutions results in a disproportionation to $[Zn(H_2O)_6][ZnCl_4]$,[35,36] $[Zn(H_2O)_6][ZnCl_4]\cdot 3H_2O$,[35] $[(H_2O)_5ZnClZnCl_3]$[36] or $[Cl_3ZnClZn(H_2O)_4ClZnCl]_n$[37] compounds depending on the crystallization temperature. The mean Zn–Cl bond distance in the tetrachlorozincate(II) ion in the solids $[Zn(H_2O)_6][ZnCl_4]$[35,36] and $[Zn(H_2O)_6][ZnCl_4]\cdot 3H_2O$[36] are 2.271 and 2.276 Å, respectively, and in other compounds containing a $[ZnCl_4]^{2-}$ ion in the solid state, it is 2.270 Å, Table S6a (SI). The mean Zn–Cl bond distance in the $[Zn_2Cl_6]^{2-}$ ion in solid state compounds is 2.260 Å, Table S7 (SI). The Zn–O, Zn–$Cl_{terminal}$ and Zn–$Cl_{bridging}$ bond distances in the $[(H_2O)_5ZnClZnCl_3]$[36] complex in the solid state are 2.076, 2.275 and 2.469 Å, respectively. The Zn–O, Zn–$Cl_{terminal}$ and Zn–$Cl_{bridging}$ bond distances in the $[Cl_3ZnClZn(H_2O)_4ClZnCl]_n$ polymer complex ($ZnCl_2\cdot 4/3H_2O$) in the solid state are 2.023, 2.278 and 2.601 Å, respectively.[37] The precipitation from saturated aqueous zinc(II) bromide solution results in disproportionation to $[Zn(H_2O)_6][Zn_2Br_6]$.[38] The mean Zn–Br bond distance in solid compounds containing a $[Zn_2Br_6]^{2-}$ ion is 2.395 Å, Table S7 (SI). The mean Zn–Br bond distance in $[ZnBr_4]^{2-}$ complexes in the solid state is 2.410 Å, Table S6c (SI). No crystal structure determination has been reported for compounds crystallizing from saturated zinc iodide solutions.

An early LAXS study on a 27.5 mol (kg water)$^{-1}$ aqueous $ZnCl_2$ solution reported that each zinc binds three chlorides and one water and that two chloride ions are shared by two zinc ions; thus, a dimer with the composition $[Zn_2Cl_4(H_2O)_2]$ and roughly tetrahedral coordination geometry around zinc,[39] and the Zn–O and Zn–Cl bond distances are 2.05 and 2.28 Å, respectively. In more diluted solutions, 8.5 and 5.0 mol (kg water)$^{-1}$, the fraction of monomeric $[ZnCl_2(H_2O)_2]$ complexes in the solution increases with dilution.[39] In a 2.3 mol dm^{-3} aqueous zinc(II) chloride solution, the dominating species is $[ZnCl_2(H_2O)_2]$ with Zn–O and Zn–Cl bond distances of 2.05 and 2.30 Å, respectively.[40] A combined Raman spectroscopy and LAXS study on highly concentrated aqueous zinc(II) chloride solutions reports an increasing number of Zn–Cl bonds per formula unit with increasing concentration due to linking through the corners of tetrahedral $ZnCl_4$ units with the shortest Zn⋯Zn distance being 3.95 Å.[41] An early LAXS study on an aqueous solution of $ZnBr_2$ shows that the dominating species is a $[ZnBr_2(H_2O)_2]$ complex with distorted tetrahedral geometry and a Zn–Br bond distance of 2.40 Å.[42] Raman spectra of 3.5 and 10.0 mol dm^{-3} aqueous solutions of zinc bromide show the presence of zinc–bromide species with 2, 3 and 4 bromides, which indicates a larger bromide coordination number than the $Br^-:Zn^{2+}$ ratio of two, thereby sharing bromide ions of at least two zinc(II) ions.[43] A combined Raman spectroscopy and LAXS study on 7.57 and 2.51 mol dm^{-3} aqueous solutions of zinc bromide reports the simultaneous presence of $[Zn(H_2O)_6]^{2+}$, $[ZnBr_2(H_2O)_2]$, $[ZnBr_3(H_2O)]^-$ and $[ZnBr_4]^{2-}$ complexes with a Zn–O bond distance of 2.10 in the hydrated zinc(II) ion and Zn–Br bond distances of 2.386, 2.386 and 2.408 Å in the $[ZnBr_2(H_2O)_2]$, $[ZnBr_3(H_2O)]^-$ and $[ZnBr_4]^{2-}$ complexes, respectively;[44] these Zn–Br bond distances in the $[ZnBr_2(H_2O)_2]$, $[ZnBr_3(H_2O)]^-$ and $[ZnBr_4]^{2-}$ complexes can be compared with reported bond distances for these complexes in the solid state, 2.351, 2.375 and 2.410 Å, respectively, Table S6 (SI). A LAXS study on concentrated aqueous zinc(II) bromide solutions in a temperature range of 25–100 °C shows that the Zn–Br bond distance becomes shorter and that the Br–Zn–Br bond angle increases with increasing temperature.[45]

The free hydrated chloride and bromide ions hydrogen bind six water molecules in octahedral geometry in aqueous solution with mean X⋯(H)–O distances of 3.25 and 3.35 Å, respectively.[46,47]

This study aims to determine the structure of highly concentrated (close to saturation) and 1.0 mol dm^{-3} aqueous solutions of first-row transition metal chlorides and bromides. Most of these structures were determined more than 40 years ago, and in many cases, with scattered results, *vide supra*. With improved instrumentation, it is now possible to collect more accurate data with improved resolution. In addition, EXAFS data are collected on 1.0 mol dm^{-3} solutions in order to make composition and structure comparisons between solutions with deficit and sufficient amounts of water for the complete hydration of the ions.

Experimental

Chemicals

Anhydrous manganese(II) bromide, $MnBr_2$, cobalt(II) chloride, $CoCl_2$, cobalt(II) bromide, $CoBr_2$, nickel(II) chloride, $NiCl_2$, nickel(II) bromide, $NiBr_2$, copper(II) chloride, $CuCl_2$, copper(II) bromide, $CuBr_2$, zinc(II) chloride, $ZnCl_2$, and zinc(II) bromide, $ZnBr_2$ (all Aldrich, 99.9%) were used as supplied.

Solutions

Stock solutions were prepared by dissolving a weighed amount (with 0.1 mg precision) of the respective salt in Millipore-filtered deionized water with a resistivity >18.2 MΩ cm. The concentrations and absorption coefficients of the solutions used in the LAXS and EXAFS measurements are summarized in Table 2.

Table 2 Compositions (in mol dm^{-3}), densities (ρ/g cm^{-3}), and linear absorption coefficients of Mo-Kα radiation (μ/cm^{-1}) of the aqueous solutions used in the LAXS (L) and EXAFS (E) experiments, including the concentrations of metal and halide ions, $c_M{}^{2+}$ and $c_X{}^-$, the concentration of water, c_{H_2O}, number of water molecules per dissolved ML_2, c_{H_2O}/c_{ML_2}, and theoretical c_{H_2O}/c_{ML_2} ratio required for full hydration of the ions at complete dissociation in the studied salts

Solute	$c_M{}^{2+}$	$c_X{}^-$	c_{H_2O}	c_{H_2O}/c_{ML_2}	$c_{H_2O}/c_{ML_2\ (req)}$	ρ	μ	Method
$MnBr_2$	3.600	7.200	47.444	13.18	30	1.6278	53.803	L
$CoCl_2$	1.001	2.002	53.666	53.60	30	1.0968	4.483	E
$CoBr_2$	3.202	6.404	49.146	15.35	30	1.5730	49.379	L, E
$NiCl_2$	1.001	2.002	54.485	54.44	30	1.1131	4.732	E
$NiCl_2$	4.985	9.970	47.007	9.43	30	1.4929	18.685	E
$NiBr_2$	1.000	2.000	53.837	53.84	30	1.1884	16.657	E
$NiBr_2$	4.800	9.600	52.011	10.84	30	1.9858	75.471	L, E
$CuCl_2$	1.001	2.002	54.389	54.386	30	1.1137	5.227	E
$CuCl_2$	3.590	7.180	44.264	12.33	26	1.3519	15.130	E
$CuBr_2$	1.000	2.000	53.943	53.94	26	1.1951	17.159	E
$CuBr_2$	5.670	11.340	32.139	5.67	30	1.9588	97.118	L, E
$ZnCl_2$	11.817	23.634	22.292	1.89	30	2.0121	52.836	L
$ZnBr_2$	5.600	11.200	42.433	7.58	30	2.0255	92.620	L, E

Large angle X-ray scattering

A large-angle θ–θ diffractometer was used to measure the scattering of Mo Kα radiation, λ = 0.7107 Å, from the free surface of the aqueous solutions. The solutions were placed in a Teflon cuvette inside a radiation shield with beryllium windows. After monochromatization of the scattered radiation using a focusing LiF crystal, the intensity was measured at 450 discrete points in the range $1 < \theta < 65°$ (the scattering angle is 2θ). The divergence of the primary X-ray beam was limited to 1° or $\frac{1}{4}$° slits for different θ regions, with overlapping parts in some regions for scaling purposes. A total of 100 000 counts were accumulated at each angle, and the angular range was scanned twice, corresponding to a statistical uncertainty of about 0.3%. All data treatment was carried out using the KURVLR program,[48] and the data treatment procedure was described in detail elsewhere.[49] The experimental intensities were normalized to a stoichiometric unit of volume containing one metal atom, using the scattering factors f for neutral atoms, including corrections for anomalous dispersion, $\Delta f'$ and $\Delta f''$,[50] and values for Compton scattering.[51,52] For a better alignment of the intensity function, a Fourier back-transformation was applied to eliminate spurious (unrelated to any interatomic distances) peaks below 1.2 Å in the radial distribution function (RDF).[53] Least-squares refinements of the model parameters were performed by applying the STEPLR program[54] to minimize the error square sum $U = \sum w(s)\cdot[i_{exp}(s) - i_{cal}(s)]^2$, where $s = 4\pi\cdot\sin(\theta)/\lambda$. The refinements of the structural parameters in the studied solutions are made within complete complex models, as presented in Table 3. This means that all interatomic distances and temperature coefficients within the proposed model are included in the refinements, as long as free rotation around a bond does not cause variation in the interatomic distance.

EXAFS

Cobalt, nickel, copper, zinc and bromine K-edge X-ray absorption data were collected in transmission mode at ambient temperature at the Balder beamline at the MAX IV Laboratory, Lund University, Sweden.[13,55] MAX IV operated at 3 GeV with a maximum current of 250 mA. A Si[111] double crystal monochromator was used, and higher harmonics were rejected by the vertical collimating mirror before, and the focusing mirror after the monochromator; for the bromide measurements, the mirrors were Pt coated. The solutions were kept in cells made of thin Kapton foil windows, 1–2 mm Teflon spacers and titanium frames. The concentrations of the studied solutions are listed in Table 2. The X-ray absorption spectra were energy calibrated using cobalt, nickel, copper and zinc metal foils and solid potassium bromide as internal standards with the first inflection point of the K-edge absorption defined as 7709.5, 8331.6, 8980.3, 9660.7 and 13 474 eV, respectively.[56] The experimental data were treated using standard procedures for pre-edge subtraction, spline removal and Fourier transformation by applying the program package EXAFSPAK.[57] *Ab initio* calculated EXAFS parameters, generated by the program FEFF v. 7.0,[58] were used in the curve-fitting procedure.

Results and discussion

Manganese(II) bromide

The RDF from LAXS data of an almost saturated (3.20 mol dm^{-3}) aqueous solution of $MnBr_2$ shows five peaks at 2.2, 2.7, 3.3, 4.0 and 4.75 Å, Fig. 1. The first two peaks correspond to the Mn–O and Mn–Br bond distances in the hydrated manganese(II) bromide complex, refined to 2.180(10) and 2.661(5) Å, respectively, Table 3. The peak at 3.3 Å corresponds to the mean Br(···H)–O distance in the coordinated hydrated bromide ions in the $[MnBr_2(H_2O)_4]$ complex. The peak at 3.9 Å corresponds to the Br···Br distance in the $[MnBr_2(H_2O)_4]$ complex, refined to 3.897(8) Å, which gives a mean Br–Mn–Br bond angle of 94.1(6)°, showing that the $[MnBr_2(H_2O)_4]$ complex has *cis*-configuration. The peak at 4.75 Å corresponds to the O···O distances in the octahedrally hydrated bromide ion and the linear Br–(Mn)–O distances in the *cis*-$[MnBr_2(H_2O)_4]$ complex. The $Mn(-O_I-H)\cdots O_{II}$ distance was

Table 3 Mean bond distances (d/Å), number of distances (N), and temperature coefficients (b/Å^2) in the LAXS studies of aqueous solutions saturated with metal chloride and bromide salts at room temperature. The estimated standard deviations given within parentheses include only statistical errors

Species	Interaction	N	d	b
3.20 mol dm^{-3} $MnBr_2$ in water, hydrated inner-sphere cis-manganese(II) bromide complex				
[*cis*-$Mn(H_2O)_4(Br(H_2O)_4)_2$]	Mn–O	4	2.180(5)	0.0086(6)
	Mn–Br	2	2.661(2)	0.0075(3)
	cis-Br···Br	1	3.897(4)	0.0128(7)
	cis-Br···O	6	3.440(5)	0.0114(7)
	trans-Br···O	2	4.841(7)	0.0161(9)
	trans-O···O	1	4.360(10)	0.0172(12)
	Br(···H)–O	4	3.298(7)	0.0166(5)
[*cis*-$Mn(Br_2(OH_2)_4)\cdots(OH_2)_8$]	Mn(–O_I···H)–O_{II}	8	4.34(2)	0.033(3)
Water bulk	$O_{aq}\cdots O_{aq}$	2	2.892(7)	0.018(2)
3.60 mol dm^{-3} $CoBr_2$ in water, inner– and outer–sphere cobalt(II) bromide complex				
[$Co(H_2O)_5(Br(H_2O)_4)$]	Co–O	5	2.093(6)	0.0096(6)
	Co–Br	1	2.621(3)	0.0075(3)
	cis-Br···O	4	3.354	0.0122(7)
	trans-Br···O	1	4.714	0.0171(9)
	cis-O···O	9	2.960	0.0136(9)
	trans-O···O	2	4.186	0.0192(12)
	Br(···H)–O	4	3.252(5)	0.0162(4)
	Co($(OH_2)_5$)···Br	1	4.336(11)	0.028(2)
[$Co(Br(OH_2)_5)\cdots(OH_2)_8$]	Co(–O_I···H)–O_{II}	10	4.28(2)	0.031(3)
Water bulk	$O_I\cdots O_{II}/O_{aq}\cdots O_{aq}$	2	2.891(6)	0.020(2)
4.80 mol dm^{-3} $NiBr_2$ in water, partial inner-sphere nickel(II) bromide complex				
[$Ni(H_2O)_{5.8}Br_{0.2}$]	Ni–O	5.8	2.075(5)	0.0060(4)
	Ni–Br	0.2	2.57(2)	0.018(4)
	cis-Br···O	0.8	3.30	0.019(4)
	trans-Br···O	0.2	4.65	0.024(5)
	cis-O···O	11.2	2.960	0.0085(6)
	trans-O···O	2.8	4.186	0.012(5)
	Ni($(OH_2)_{5.8}$)···Br	1.8	4.390(6)	0.0277(12)
$Br(H_2O)_5^-$	Br(···H)–O	5	3.283(5)	0.0166(5)
[$Ni(Br_{0.2}(OH_2)_{5.8})\cdots(OH_2)_{11.6}$]	Ni(–O_I···H)–O_{II}	11.6	4.217(9)	0.034(2)
Water bulk	$O_I\cdots O_{II}/O_{aq}\cdots O_{aq}$	2	2.910(6)	0.020(2)
5.67 mol dm^{-3} $CuBr_2$ in water, hydrated inner-sphere cis-copper(II) bromide complex				
[$Cu(H_2O)_2(Br_2(H_2O)_{10})]_n$	Cu–O	2.0	1.985(5)	0.0091(4)
	Cu–Br	2.0	2.465(2)	0.0042(2)
	Cu···O	1.0	2.82(2)	0.009(2)
	cis-Br–(Cu)–Br	1.0	3.476(4)	0.0084(4)
	trans-Br–(Cu)–O	2.0	4.450(7)	0.0133(6)
	cis-O–(Cu)–O	1.0	2.807(7)	0.0129(7)
	Cu···Cu/Br	2.0	5.618(10)	0.034(2)
	Cu···Br	4.0	6.168(7)	0.036(2)
	Br(···H)–O	5	3.342(5)	0.0137(7)
[$Cu(Br_2(OH_2)_2)\cdots(OH_2)_4$]	Cu(–O–H)···O_{II}	4.0	4.131(5)	0.0191(8)
Water bulk	$O_I\cdots O_{II}$	1.25	2.85(3)	0.035(7)
5.60 mol dm^{-3} $ZnBr_2$ in water, dimeric zinc(II) bromide complex				
[$Zn_2Br_4(H_2O)_2$]	Zn–Br_t	1.0	2.272(2)	0.0031(3)
	Zn–Br_b	2.0	2.374(1)	0.0029(2)
	$Br_t\cdots Br_b$	2.0	3.923(2)	0.0096(3)
	$Br_b\cdots Br_b$	0.5	4.023(9)	0.0115(13)
	Zn···Zn	0.5	2.634(9)	0.0153(15)
	Zn–O	1.0	2.061(12)	0.0081(12)
$Br(H_2O)_3^-$	Br(···H)–O	2.5	3.333(9)	0.033(2)
Water bulk	$O_I\cdots O_{II}/O_{aq}\cdots O_{aq}$	2	2.874(9)	0.0137(17)
11.82 mol dm^{-3} $ZnCl_2$ in water, dimeric zinc(II) chloride complex				
[Zn_2Cl_4]	Zn–Cl_b	2.0	2.225(1)	0.0046(2)
	Zn–Cl_t	1.0	2.130(2)	0.0059(3)
	$Cl_t\cdots Cl_b$	2.0	3.792(5)	0.0102(7)
	$Cl_b\cdots Cl_b$	0.5	3.87(2)	0.008(3)
	Zn···Zn	0.5	2.51(1)	0.016(1)

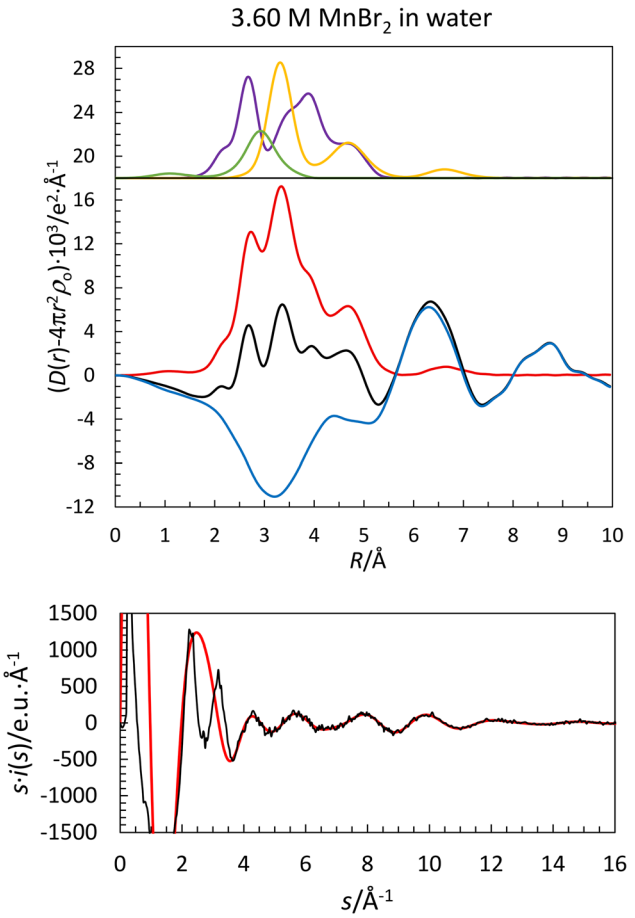

Fig. 1 (Top) LAXS radial distribution curves for a 3.60 mol dm^{-3} aqueous solution of manganese(II) bromide. Separate model contributions (offset: 18) of the hydrated *cis*-dibromomanganese(II) complex (purple line), the hydrated bromide ion (yellow line) and aqueous bulk (green line). (Middle) Experimental RDF: $D(r) - 4\pi r^2\rho_0$ (black line); sum of model contributions (red line); difference (blue line). (Bottom) Reduced LAXS intensity functions $s{\cdot}i(s)$ (black line); model $s{\cdot}i_{calc}(s)$ (red line).

refined to 4.34(5) Å, which is slightly longer than that in the hydrated manganese(II) ion, 4.26(2) Å.[11] This increase in Mn(–O_I–H)···O_{II} distance is caused by the reduced charge density and thereby reduced polarizability on manganese due to the partly covalent bonding character of the Mn–Br bonds. Therefore, the O_I(–H)···O_{II} distance between the first and second hydration shells increases to *ca.* 2.89 Å, compared to 2.79 Å in the hydrated manganese(II) ion.[11] This shows that significant complex formation takes place in highly concentrated aqueous manganese(II) bromide solution in contrast to dilute aqueous solution, Table S1a (SI). The bromide ions in the *cis*-$[MnBr_2(H_2O)_4]$ complex are hydrated by 4–5 water molecules with a mean Br(···H)–O distance of 3.30(2) Å, Table 3. The complex observed in saturated aqueous solution is identical to the complex in the solid state,[59,60] Fig. 2 and Table S2 (SI), as reported in previously studied concentrated aqueous solutions.[15,16] A dimeric $[(H_2O)_4MnBr_2Mn(H_2O)_4]$ complex is reported in the solid state,[61] but such a complex could not be

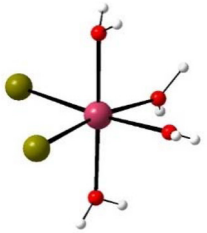

Fig. 2 Structure of the *cis*-$[MnBr_2(H_2O)_4]$ complex.

detected in the studied aqueous solution. The *cis*-configuration is also the most common in the solid state for the manganese(II)–chloride system, α-$[MnCl_2(H_2O)_4]$. The structures of the complexes in *trans*-configuration, β-$[MnBr_2(H_2O)_4]$ and β-$[MnCl_2(H_2O)_4]$, have layered structures,[62,63] Table S2 (SI). We collected EXAFS data on 1.0 mol dm^{-3} and highly concentrated aqueous manganese(II) chloride and bromide solutions; however, due to the presence of large glitches in the data sets, it was not possible to make a proper data treatment.

Cobalt(II) chloride and bromide

Cobalt(II) forms very weak complexes with the halide ions in dilute aqueous solution, Table S1b (SI), indicating that solvent-shared ion pairs are formed. The EXAFS spectra of aqueous solutions of 1.0 mol dm^{-3} $CoCl_2$ and 0.2 mol dm^{-3} $Co(ClO_4)_2$, and solid $[Co(H_2O)_6](ClO_4)_2$ are almost superimposed, Fig. 3. This shows that the inner-core structure around cobalt(II) in these samples is a regular octahedral $[Co(H_2O)_6]^{2+}$ complex. The minor differences at low *k*-values may indicate differences in the second coordination sphere in the aqueous solutions, and the presence of perchlorate ions in the solid. Solid hexaaquacobalt(II) perchlorate has the same phase as the aqueous solutions but slightly higher amplitude, Fig. 3, which indicates a somewhat narrower Co–O bond distance distribution in the solid state than in aqueous solution. The superimposing EXAFS spectra show that cobalt(II) does not bind chloride ions as inner-sphere complexes in aqueous solutions less concentrated than 1.0 mol dm^{-3}. The Co–O bond distance in the

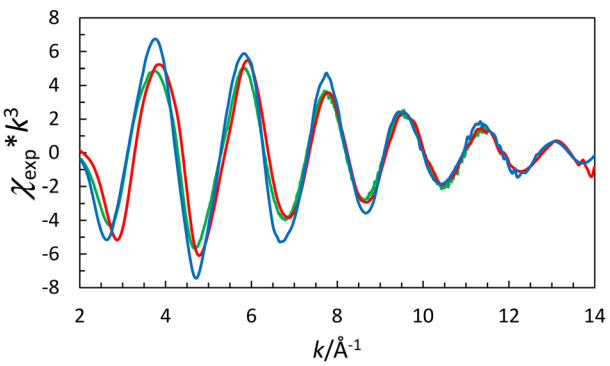

Fig. 3 Superimposed EXAFS data of aqueous solutions of 1.00 mol dm^{-3} cobalt(II) chloride (green line), and 0.20 mol dm^{-3} cobalt(II) perchlorate (red line) and solid $[Co(H_2O)_6](ClO_4)_2$ (blue line).

1.0 mol dm^{-3} aqueous solution cobalt(II) chloride is refined to 2.073(3) Å in an octahedral $[Co(H_2O)_6]^{2+}$ complex, in agreement with the observations in solid state structures, 2.088 Å, Table S11a in ref. 11, and 2.090 Å in aqueous solution.[11] The fits of the EXAFS raw data and the Fourier transforms are shown in Fig. 4 and 5, respectively. EXAFS cannot distinguish the presence of any solvent-shared ion-pairs or a second hydration shell due to long distances and large Debye–Waller factor coeffcients.[64]

The RDF of an almost saturated (3.60 mol dm^{-3}) aqueous solution of $CoBr_2$ shows three peaks at 2.1, 3.3 and 4.4 Å, and a shoulder at 2.65 Å, Fig. 6. The peak at 2.1 Å and the shoulder at 2.65 Å, refined to 2.093(12) and 2.621(6) Å, respectively, correspond to the Co–O and Co–Br bond distances in a hydrated monobromocobalt(II) complex. The peak at 3.3 Å corresponds to the mean Br···(H–)O distances in the hydrated bromide ions in the first and second coordination shells. The peak at 4.3 Å has two contributions: the Co(–O–H)···Br distance in the second coordination shell, refined to 4.34(3) Å, and the second hydration sphere, $Co(-O_I-H)\cdots O_{II}$, refined to 4.28(5) Å, Table 3. The second hydration shell is at a significantly longer distance than in the hydrated cobalt(II) ion, 4.07 (2) Å.[11] The cobalt(II)–bromide bond has a partly covalent character due to the soft bonding properties of the bromide ion, reducing the charge density and polarizability of cobalt(II). This results in a longer $(Co-)O_I(-H)\cdots O_{II}$ distance, *ca.* 2.89 Å, and a $Co-O_I(-H)\cdots O_{II}$ bond angle of *ca.* 117°, compared to 112° in the hydrated cobalt(II) ion.[11] The observed distances and intensities of Co–O, Co–Br and Co(–O–H)···Br result in a complex, wherein, on average, approximately one bromide ion is bound as an inner-sphere complex and the other bromide ion forms a solvent-shared ion-pair, $[CoBr(H_2O)_4(H_2O)\cdots Br(H_2O)_5]$. This shows that cobalt(II) forms weaker bromide complexes than manganese(II) in highly concentrated aqueous solution, *ca.* 3.5 mol dm^{-3}, as well as in dilute aqueous solution, Table S1 (SI). The Co–O and Co–Br bond distances in the first coordination shell are in close agreement with those observed in the *trans*-$[CoBr_2(H_2O)_4]$ complex in the solid state,[65–67] Table S3 (SI). The results obtained in this study are in good agreement with a previous LAXS study reporting $[CoBr_n(H_2O)_{6-n}]^{(2-n)+}$ complexes with n = 0.3 and 0.6 in 2.85 and 4.25 mol dm^{-3} aqueous cobalt(II) bromide solutions, respectively.[68]

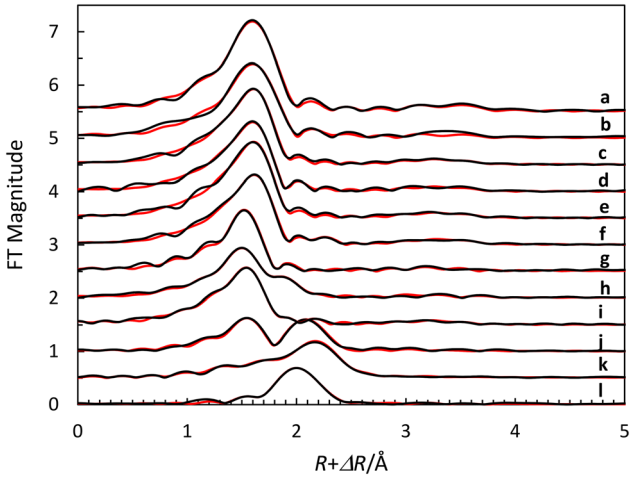

Fig. 5 Fit of Fourier transforms of raw EXAFS data of (a) aqueous solutions of 1.00 mol dm^{-3} cobalt(II) chloride, offset: 5.5; (b) saturated cobalt (II) bromide, offset: 5.0; (c) 1.00 mol dm^{-3} nickel(II) chloride, offset: 4.5; (d) saturated nickel(II) chloride, offset: 4.0; (e) 1.00 mol dm^{-3} nickel(II) bromide, offset: 3.5; (f) saturated nickel(II) bromide, offset: 3.0; (g) 1.00 mol dm^{-3} copper(II) chloride, offset: 2.5; (h) saturated copper(II) chloride, offset: 2.0; (i) 1.00 mol dm^{-3} copper(II) bromide, offset: 1.5; (j) saturated copper(II) bromide, offset: 1.0; (k) saturated zinc(II) bromide (zinc edge data), offset: 0.5; and (l) saturated zinc(II) bromide (zinc edge data), no offset.

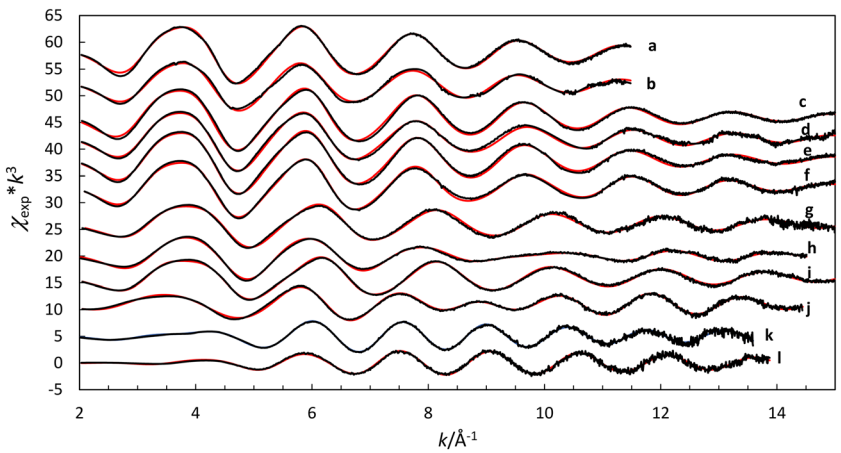

Fig. 4 Fit of raw EXAFS data of aqueous solutions of (a) 1.00 mol dm^{-3} cobalt(II) chloride, offset: 54; (b) saturated cobalt(II) bromide, offset: 50; (c) 1.00 mol dm^{-3} nickel(II) chloride, offset: 46; (d) saturated nickel(II) chloride, offset: 42; (e) 1.00 mol dm^{-3} nickel(II) bromide, offset: 38; (f) saturated nickel(II) bromide, offset: 34; (g) 1.00 mol dm^{-3} copper(II) chloride, offset: 26; (h) saturated copper(II) chloride, offset: 19; (i) 1.00 mol dm^{-3} copper(II) bromide, offset: 17; (j) saturated copper(II) bromide, offset: 10; (k) saturated zinc(II) bromide, offset: 5; and (l) saturated zinc(II) bromide, no offset.

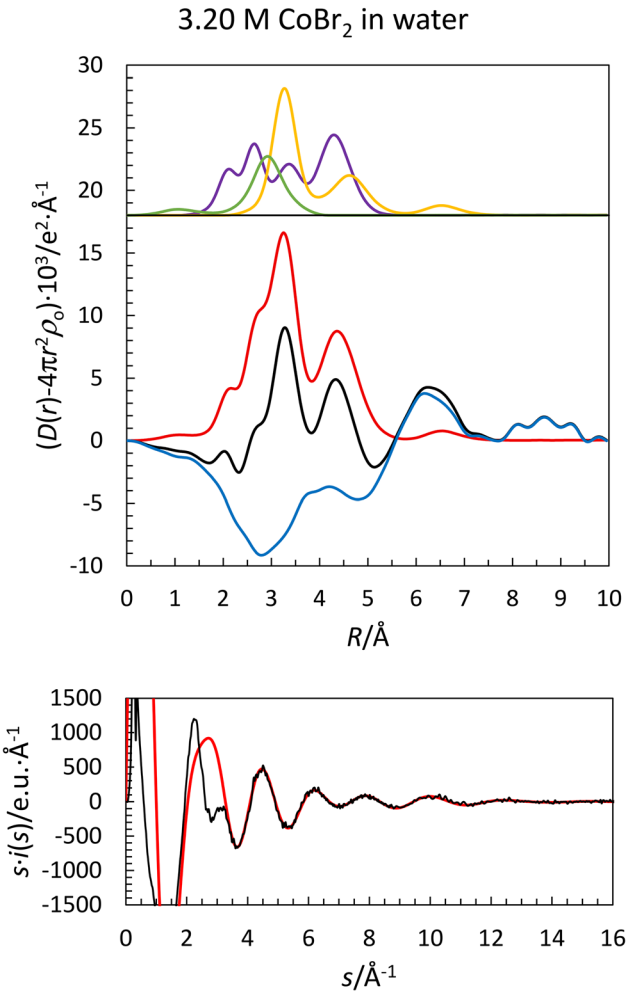

Fig. 6 (Top) LAXS radial distribution curves for a 3.20 mol dm^{-3} aqueous solution of cobalt(II) bromide. Separate model contributions (offset: 18) of the hydrated monobromocobalt(II) complex (purple line), the hydrated bromide ion (yellow line) and aqueous bulk (green line). (Middle) Experimental RDF: $D(r) - 4\pi r^2\rho_0$ (black line); sum of model contributions (red line); difference (blue line). (Bottom) Reduced LAXS intensity functions $s\cdot i(s)$ (black line); model $s\cdot i_{calc}(s)$ (red line).

The EXAFS data of the almost saturated cobalt(II) bromide solution fully support the results from the LAXS study with Co–O and Co–Br bond distances of 2.077(3) and 2.62(2) Å, Table 4. The fits of the experimental raw data and the Fourier transform are shown in Fig. 4 and 5. The structure of the dominating complex in a saturated aqueous cobalt(II) bromide solution, $[CoBr(H_2O)_4(H_2O)\cdots Br(H_2O)_5]$, has similarities with the *trans*-$[CoBr_2(H_2O)_4]$ complex in the solid state. At crystallization, the water molecules in the second hydration sphere are transferred to the aqueous bulk, as the hydrogen bonds between the first and second hydration shells are weaker than the hydrogen bonds in the aqueous bulk,[11] *vide supra*, and the bromide ion in the second hydration replaces the water molecule *trans* to the other bromide ion in the first coordination sphere. As cobalt(II) formed weaker complexes with chloride than bromide in aqueous solution (Table S1b) and no inner-sphere complex formation with chloride was observed in the 1.0 mol dm^{-3} solution, the outcome of a structure determination of a 1.0 mol dm^{-3} cobalt(II) bromide solution was predictable, and no data were collected.

Nickel(II) chloride and bromide

Nickel(II) forms weak complexes with halide ions in dilute aqueous solution, Table S1c (SI). This is proven by the superimposing EXAFS spectra of 1.0 mol dm^{-3} aqueous solutions of nickel chloride and bromide, 0.200 mol dm^{-3} nickel perchlorate and solid $[Ni(H_2O)_6](ClO_4)_2$, Fig. 7. The Ni–O bond distances in the 1.0 mol dm^{-3} aqueous solutions of nickel(II) chloride and bromide are refined to 2.042(3) Å in octahedral $[Ni(H_2O)_6]^{2+}$ complexes, which agrees with the observations in solid state structures (2.055 Å; Table S12a in ref. 11) and with those in an aqueous solution (2.057 Å).[11] The EXAFS spectra of saturated (4.98 mol dm^{-3}) nickel(II) chloride and (4.80 mol dm^{-3}) nickel(II) bromide differ slightly from those of 1.0 mol dm^{-3} one, especially around $k \approx 7$ Å^{-1}, Fig. 7, due to the partial presence of halide ions in the inner coordination sphere. The Ni–Cl and Ni–Br bond distances are refined to 2.37(1) and 2.497(6) Å, respectively, and the Ni–O bond distances to 2.04(1) Å in both complexes, which are slightly shorter than in the $[NiCl_2(H_2O)_4]$ and $[NiBr_2(H_2O)_4]$ complexes in the solid state, Table S4 (SI).

The RDF of the 4.80 mol dm^{-3} aqueous solution of $NiBr_2$ shows three peaks at 2.05, 3.3 and 4.4 Å, and a shoulder at 2.6 Å, Fig. 8. The peak at 2.05 Å and shoulder at 2.6 Å, refined to 2.075(10) and 2.57(2) Å, respectively, correspond to the Ni–O bond distances in the hydrated nickel(II) ion and the hydrated monobromonickel(II) complex, and the Ni–Br bond distance in the hydrated monobromonickel(II) complex. The peak at 3.3 Å is related to Br(···H)–O distances in the hydrated bromide ions in the first and second hydration shells of the monobromonickel(II) complex. The peak at 4.4 Å has two contributions: the Ni(–O–H)···Br distance in an outer-sphere bromide complex, refined to 4.39(2) Å, and the second hydration sphere, refined to 4.22(3) Å, Table 3. The second hydration shell is at a significantly longer distance than that in the hydrated nickel(II) ion, 3.98 (2) Å.[11] The bound bromide ions reduce charge density and polarizability on nickel, resulting in a longer $O_I(–H)\cdots O_{II}$ distance, *ca.* 2.91 Å. This gives a $Ni–O_I(–H)\cdots O_{II}$ bond angle of *ca.* 115° compared to 110° in the hydrated nickel(II) ion.[11] The contribution from the Ni–Br bond in the RDF indicates, on average, *ca.* 0.2 Ni–Br bonds. The observed Ni–O, Ni–Br and Ni(–O–H)···Br distances result in a complex where, on average, *ca.* 0.2 bromide ions are bound as an inner-sphere complex and the remaining 1.8 bromide ions as solvent-shared ion-pairs. Thus, *ca.* 80% of the nickel content is present as hydrated nickel(II) ions with two bromide ions in the second coordination shell, $[Ni(H_2O)_6\cdots(Br(H_2O)_5)_2]$, and *ca.* 20% as monobromonickel(II) complexes with one bromide in the second coordination shell, $[NiBr(H_2O)_5\cdots(Br(H_2O)_5)]$, mean $[NiBr_n(H_2O)_{6-n}\cdots(Br(H_2O)_5)_{2-n}]$, n = 0.2. The weak complex formation of nickel(II)–halide complexes is further shown by the fact that nickel(II) iodide crystallizes from aqueous solution as

Table 4 Mean bond distances (d/Å), Debye–Waller factors (σ^2), number of distances (N), and the shift in the threshold energy (ΔE_0/eV) of 1.0 mol dm^{-3} and saturated aqueous solutions of cobalt(II), nickel, copper(II), and zinc(II) as determined by EXAFS at room temperature

Interaction	N	d	σ^2	ΔE_0	$S_0{}^2$	F
1.00 mol dm^{-3} cobalt(II) chloride, k = 2.0–11.5 Å^{-1}						
Co–O	6	2.073(1)	0.0067(1)	−7.7(1)	0.865(4)	8.45
MS	3 × 6	4.146	0.0121(6)			
Highly concentrated (3.20 mol dm^{-3}) cobalt(II) bromide, k = 2.0–11.5 Å^{-1}						
Co–O	5.0	2.077(1)	0.0071(1)	−7.2(1)	0.885(8)	15.05
MS	3 × 5	4.154	0.021(1)			
Co–Br	1.0	2.616(8)	0.022(2)			
1.0 mol dm^{-3} nickel(II) chloride, k = 2.0–15.0 Å^{-1}						
Ni–O	6	2.042(1)	0.0060(2)	−9.4(1)	0.898(5)	10.14
MS	3 × 6	4.084	0.0092(6)			
Highly concentrated (4.98 mol dm^{-3}) nickel(II) chloride, k = 2.0–15.0 Å^{-1}						
Ni–O	5.5	2.040(3)	0.0061(2)	−9.6(1)	0.904(8)	15.21
MS	3 × 6	4.080	0.0094(7)			
Ni–Cl	0.5	2.366(3)	0.0066(2)			
1.0 mol dm^{-3} nickel(II) bromide, k = 2.0–15.0 Å^{-1}						
Ni–O	6	2.042(1)	0.0061(1)	−9.3(1)	0.910(6)	13.25
MS	3 × 6	4.084	0.0095(8)			
Highly concentrated (4.80 mol dm^{-3}) nickel(II) bromide, k = 2.0–15.0 Å^{-1}						
Ni–O	5.8	2.043(1)	0.0058(1)	−9.3(3)	0.873(5)	11.99
MS	3 × 6	4.087	0.0079(6)			
Ni–Br	0.2	2.497(2)	0.0047(2)			
1.0 mol dm^{-3} copper(II) chloride, k = 2.0–14.5 Å^{-1}						
Cu–O	4	1.952(2)	0.0045(2)	−11.5(4)	0.76(2)	24.14
MS	3 × 4	3.903	0.0082(15)			
Cu–O_{ax1}	1	2.073(14)	0.0069(2)			
Cu–O_{ax2}	1	2.56(7)	0.038(14)			
Highly concentrated (3.59 mol dm^{-3}) copper(II) chloride, k = 2.0–15.0 Å^{-1}						
Cu–O	3.4(1)	1.953(4)	0.0031(2)	−10.3(4)	0.73(3)	13.97
Cu–Cl	0.6(1)	2.288(7)	0.0066(7)			
MS	3 × 4	3.906	0.0076(10)			
Cu–O_{ax1}	1	2.076(7)	0.0037(3)			
Cu–O_{ax2}	1	2.63(2)	0.022(3)			
1.0 mol dm^{-3} copper(II) bromide, k = 2.0–15.0 Å^{-1}						
Cu–O	4	1.966(1)	0.0054(1)	−9.9(1)	0.97(1)	10.33
MS	3 × 4	3.931	0.0095(6)			
Cu–O_{ax1}	1	2.183(2)	0.0048(2)			
Cu–O_{ax2}	1	2.384(3)	0.0076(3)			
Highly concentrated (5.67 mol dm^{-3}) copper(II) bromide, k = 2.0–15.0 Å^{-1}						
Cu–Br	2.0	2.43(2)	0.0106(2)	−16.9(3)	1.20(2)	17.29
Cu–O	2.0	1.993(1)	0.0055(2)			
Cu–O_{ax1}	1.0	2.245(2)	0.0041(3)			
Cu–O_{ax2}	1.0	2.687(2)	0.0048(2)			
Cu–Br–O, 3-leg	8.0	3.81(2)	0.007(2)			
Highly concentrated (5.60 mol dm^{-3}) zinc(II) bromide, k = 2.0–14.0 Å^{-1}						
Zn K edge data						
Zn–Br_t	1.0	2.285(3)	0.0045(3)	−8.5(6)	0.78(3)	21.03
Zn–Br_b	2.0	2.388(3)	0.0049(3)			
Zn···Zn	0.5	2.702(13)	0.016(2)			
Zn–O	1.0	2.04(5)	0.0104(7)			
Br K edge data						
Br_t–Zn	0.5	2.265(7)	0.0112(6)	−20.6(5)	1.03(4)	22.43
Br_b–Zn	2.0	2.369(2)	0.0049(2)			
Br_t···Br_b	2.0	3.925(10)	0.023(2)			
Br_b···Br_b	0.5	4.10(2)	0.014(3)			

a $[Ni(H_2O)_6]I_2$ salt.[69] The Ni–Br and Ni–O bond distances are in close agreement with those observed in the $[NiBr(H_2O)_5]^+$ complex[24] and the *trans*- and *cis*-$[NiBr_2(H_2O)_4]$ complexes in solid state,[70–74] Table S4 (SI). This result is in good agreement with a previous LAXS study reporting $[NiBr_n(H_2O)_{6-n}]^{(2-n)+}$ complexes with n = 0.18, 0.47 and 0.68 in 2.01, 4.06 and 4.85 mol dm^{-3} aqueous nickel(II) bromide solutions.[28] The structure of the bromide complex in a saturated aqueous nickel(II) bromide solution, $[NiBr(H_2O)_5(\cdots Br(H_2O)_5)]$, has similarities with the *cis*- or *trans*- $[NiBr_2(H_2O)_4]$ complexes in the solid state, Table S4 (SI). At crystallization, the second hydration sphere is transferred to the aqueous bulk, and the bromide ions in the second hydration shell replace the water molecules in the first coordination sphere.

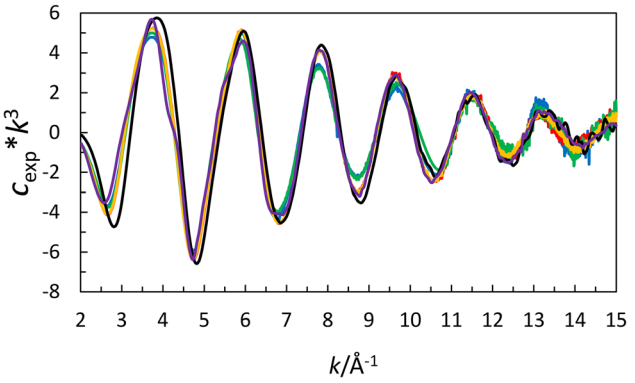

Fig. 7 Comparison of EXAFS spectra of the hydrated nickel(II) ion in 1.00 mol dm^{-3} nickel(II) chloride (yellow line), 1.00 mol dm^{-3} nickel(II) bromide (red line), 4.98 mol dm^{-3} nickel chloride (green line), 4.80 mol dm^{-3} nickel bromide (blue line), 0.200 mol dm^{-3} nickel(II) trifluoromethanesulfonate (purple line) and solid [nickel$(H_2O)_6$]$(ClO_4)_2$ (black line).

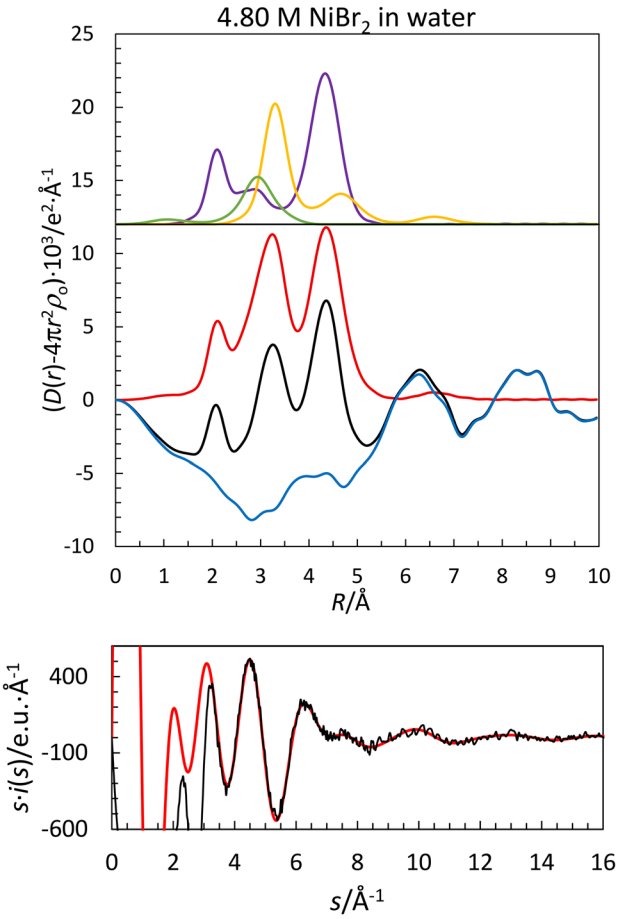

Fig. 8 (Top) LAXS radial distribution curves for a 4.80 mol dm^{-3} aqueous solution of nickel(II) bromide. Separate model contributions (offset: 12) of the hydrated nickel(II) and bromonickel(II) complexes (purple line), the hydrated bromide ion (yellow line) and aqueous bulk (green line). (Middle) Experimental RDF: $D(r) - 4\pi r^2\rho_0$ (black line); sum of model contributions (red line); difference (blue line). (Bottom) Reduced LAXS intensity functions $s\cdot i(s)$ (black line); model $s\cdot i_{calc}(s)$ (red line).

Copper(II) chloride and bromide

The hydrated copper(II) ion binds six water molecules in a Jahn–Teller distorted octahedral configuration with the two water molecules in the elongated axial positions at significantly different Cu–O bond distances in aqueous solution.[13,14] Copper(II) forms weak complexes with chloride and bromide ions in aqueous solution most likely forming solvent-shared ion-pairs, Table S1d (SI). The raw EXAFS spectra of 1.0 mol dm^{-3} aqueous solutions of copper(II) chloride and bromide, a 0.19 mol dm^{-3} aqueous copper(II) trifluoromethanesulfonate solution and solid [$Cu(H_2O)_6$]$(ClO_4)_2$ are superimposed, showing that they have very similar structures in the first coordination sphere, Fig. 9. The small differences in the raw EXAFS spectra are most likely due to the presence of a second hydration shell, which may include halide ions, in aqueous solution and of perchlorate ions in the solid. The Cu–O_{ax}, Cu–O_{eq1} and Cu–O_{eq2} bond distances in the 1.0 mol dm^{-3} aqueous solutions of copper(II) chloride and bromide are refined to 1.952(6), 2.07(3) and 2.6(2), and 1.966(3), 2.183(6) and 2.38(1) Å, respectively. This is in good agreement with the observation of the hydrated copper(II) ion in aqueous solution[13,14] and the solid state, Table S13a in ref. 11.

The fit of EXAFS data of a 3.59 mol dm^{-3} aqueous solution of copper(II) chloride shows that copper(II) binds, on average, *ca.* 0.6 chloride ions in the inner coordination sphere, Table 4 and Fig. S1 and S2 (SI). This shows that water molecules in the inner coordination sphere are exchanged for chloride ions at crystallization from aqueous solution to form *trans*-[$CuCl_2(H_2O)_2$] units, which most likely bind additional water molecules in the axial positions of tetragonally elongated (Jahn–Teller distorted) octahedral complexes.

The RDF of the LAXS data of the highly concentrated (5.87 mol dm^{-3}) aqueous solution of copper(II) bromide shows four sharp peaks at 2.45, 3.5, 4.15 and 6.15 Å, a small peak at 2.0 Å and a shoulder at 5.7 Å, Fig. 10. The peaks at 2.0 and 2.45 Å corresponds to the Cu–O and Cu–Br bond distances, which are refined to 1.985(10) and 2.465(4) Å, respectively. The

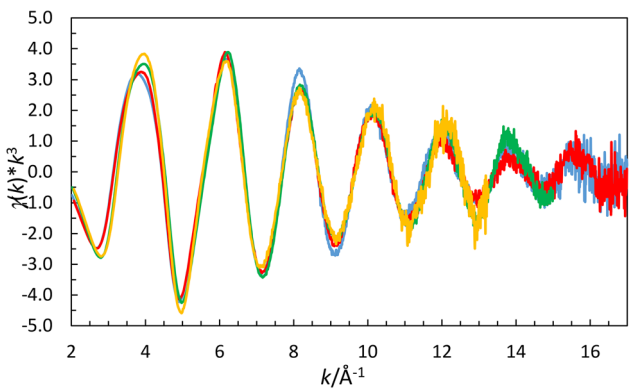

Fig. 9 Comparison of EXAFS spectra of the hydrated copper(II) ion in 1.00 mol dm^{-3} copper(II) chloride (yellow line), 1.00 mol dm^{-3} copper(II) bromide (green line), 0.190 mol dm^{-3} copper(II) trifluoromethanesulfonate (red line) and solid [$Cu(H_2O)_6$]$(ClO_4)_2$ (light blue line).

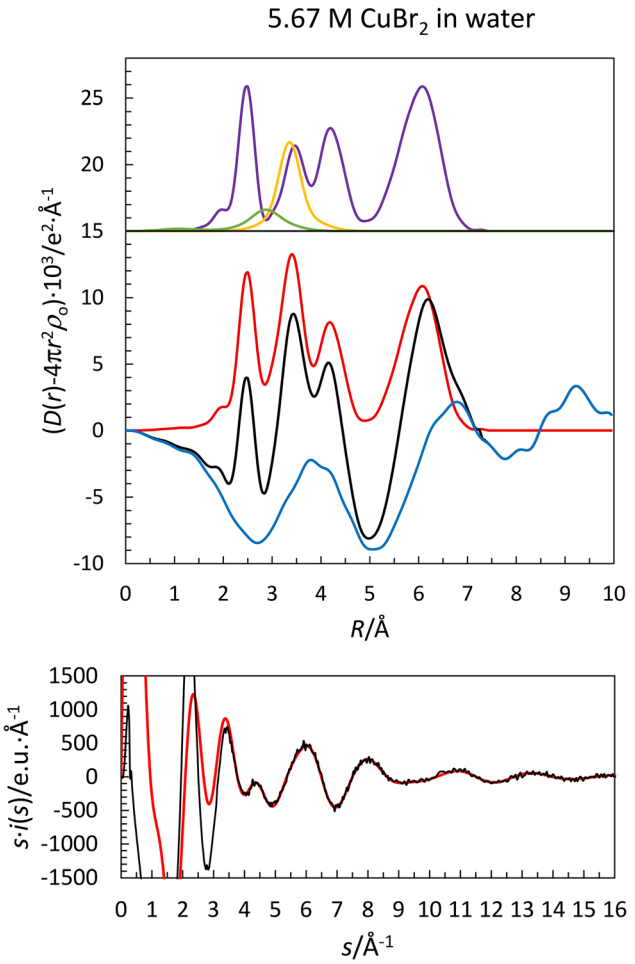

Fig. 10 (Top) LAXS radial distribution curves for a 5.67 mol dm^{-3} aqueous solution of copper(II) bromide. Separate model contributions (offset: 15) of the hydrated *trans*-dibromocopper(II) complex (purple line), the hydrated bromide ion (yellow line) and aqueous bulk (green line). (Middle) Experimental RDF: $D(r)-4\pi r^2\rho_0$ (black line); sum of model contributions (red line); difference (blue line). (Bottom) Reduced LAXS intensity functions $s\cdot i(s)$ (black line); model $s\cdot i_{calc}(s)$ (red line).

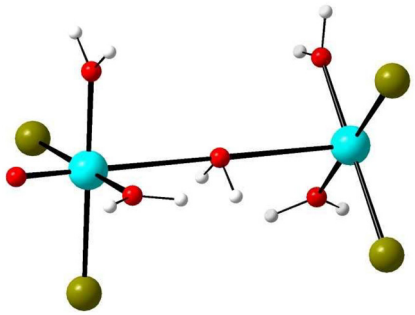

Fig. 11 Proposed structure of the copper(II) bromide complex in a saturated aqueous solution.

peak at 3.5 Å, refined to 3.476(8) Å, refers to the Br···Br distance in a square–planar *cis*-$[CuBr_2(H_2O)_2]$ unit; the Br–Cu–Br bond angle is 89.7(4)°. The peak refined to 4.13(1) Å corresponds to a second hydration sphere of the water molecules in the $[CuBr_2(H_2O)_2]$ unit. The bromide ions in the *cis*-$[CuBr_2(H_2O)_2]$ unit are hydrated by *ca.* 5 water molecules at a mean Br(···H)–O distance of 3.34(2) Å. In addition to the distances within the $[CuBr_2(H_2O)_2\cdots(H_2O)_4]$ units, an intense and very well–defined distance at 6.15 Å is observed. This shows that the *cis*-$[CuBr_2(H_2O)_2]$ units are connected most likely through an axially bound water molecule with a Cu–O bond distance of *ca.* 2.81 Å, Fig. 11. Such an arrangement yields two Cu···Cu and four Cu···Br distances per copper refined to 5.62(2) and 6.17(2) Å, respectively. This structural arrangement around copper(II) is significantly different from the solid state structures containing hydrated dibromocopper(II) complexes, all of which have a *trans*-configuration,[75–78] Table S5 (SI). This means that the observed *cis*-configuration of the $[CuBr_2(H_2O)_2]$ unit in saturated aqueous copper(II) bromide solution is unique, and a large structural reorganization takes place at the crystallization of a saturated aqueous copper(II) bromide solution. A polymeric structure with the composition $[Cu(H_2O)_2BrCu(H_2O)_4Br]_n$ has been reported in the solid state,[79] but this structure was not in agreement with the experimental LAXS data. The saturated (5.67 mol dm^{-3}) $CuBr_2$ solution has a dark brown colour and high surface tension, as observed in the small propagation of a drop on a filter paper, Fig. S3 (SI). Dilution to 5.0 mol dm^{-3} produces a less dark brown solution with larger propagation, and at 4.0 mol dm^{-3}, the solution changes colour to greenish–blue, Fig. S3 (SI). This shows that only a small dilution of the saturated $CuBr_2$ solution causes a major structural change to a complex most likely similar to the one present in the 3.59 mol dm^{-3} $CuCl_2$ solution, *vide supra*.

Zinc(II) chloride and bromide

The hydrated zinc(II) ion binds six water molecules in a regular octahedral fashion with a mean Zn–O bond distance of 2.09 Å, and 12 water molecules in the second hydration shell at a mean Zn–(O–H)···O of 4.13 Å in a dilute aqueous solution.[11] Zinc(II) forms weak complexes with chloride and bromide in dilute aqueous solutions, Table S1e (SI). Zinc chloride and bromide are highly soluble in an aqueous solution, with saturated solutions of 11.82 and 5.60 mol dm^{-3}, respectively. The RDF of the LAXS data of the saturated aqueous solution of zinc(II) bromide shows two sharp peaks at 2.35 and 3.95 Å, and a broad weak peak at 3.15 Å corresponding to interatomic O···(H–)O and Br···(H–)O distances in the aqueous bulk and the hydrated bromide ion, respectively, Fig. 12. The sharp peaks correspond to mean Zn–Br and Br–(Zn)–Br distances in a proposed dimeric $[Zn_2Br_4(H_2O)_2]$ complex refined to 2.350 and 3.924 Å, respectively, giving a mean Br–Zn–Br bond angle of 113°, which strongly indicates a distorted tetrahedral coordination around zinc, as also found in the monomeric $[ZnBr_3(H_2O)]^-$ complexes in the solid state, Table S6 (SI); the Zn–O bond distance was refined to 2.06(3) Å, Table 3. The observed Zn–Br bond distance is in agreement with the mean Zn–Br bond distance in the $[ZnBr_2(H_2O)_2]$ complexes, 2.351 Å,

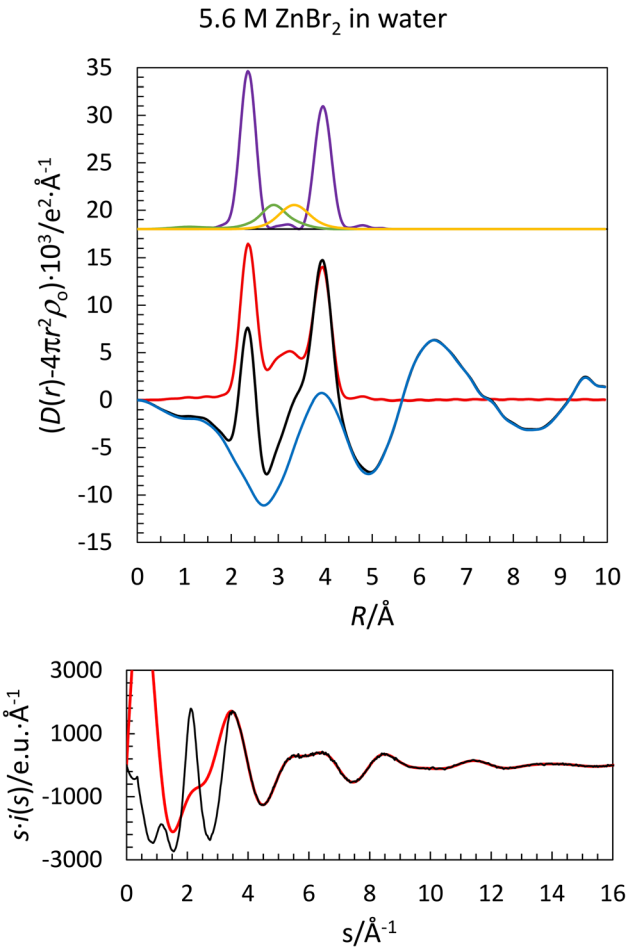

Fig. 12 (Top) LAXS radial distribution curves for a 5.60 mol dm^{-3} aqueous solution of zinc(II) bromide. Separate model contributions (offset: 18) of the hydrated tetrabromodizinc complex (purple line), the hydrated bromide ion (yellow line) and aqueous bulk (green line). (Middle) Experimental RDF: $D(r) - 4\pi r^2\rho_0$ (black line); sum of model contributions (red line); difference (blue line). (Bottom) Reduced LAXS intensity functions $s\cdot i(s)$ (black line); model $s\cdot i_{calc}(s)$ (red line).

but shorter than those in the $[ZnBr_3(H_2O)]^-$ and $[ZnBr_4]^{2-}$ complexes, 2.375 and 2.410 Å, respectively, Tables S6a and S6c (SI).

No $[Zn_2Br_4]$ or $[Zn_2Br_4(H_2O)_2]$ complexes are reported in the solid state, but the structures of numerous $[Zn_2Br_6]^{2-}$ complexes show significantly different Zn–Br bond distances to terminally and bridging bound bromide ions, 2.350 and 2.485 Å, respectively, with a mean of 2.418 Å, Table S7 (SI). By applying such a model, the terminal and bridging Zn–Br_t and Zn–Br_b bond distances were refined to 2.272(6) and 2.374(3) Å, respectively; the $Br_b\cdots Br_t$ and $Br_b\cdots Br_b$ distances to 3.923(6) and 4.023(25) Å, respectively; and the Zn⋯Zn distance to 2.63(2) Å, Table 3. These distances give Br_t–Zn–Br_b and Br_b–Zn–Br_b bond angles of 115.2 and 115.9°, respectively. The refined mean Zn–O bond distance, 2.06(3) Å, agrees with the reported mean Zn–O bond distance in $[ZnBr_3(H_2O)]^-$ complexes in the solid state, 2.047 Å, Table S6a (SI). This solution was also studied by both zinc and bromine EXAFS, resulting in

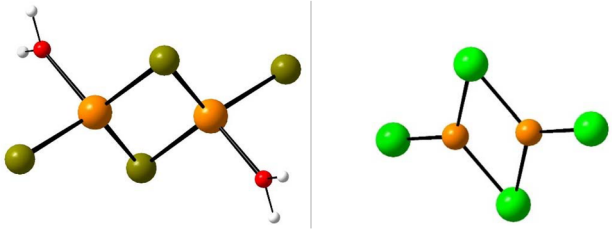

Fig. 13 Proposed structures of dimeric zinc bromide (left) and chloride complexes (right) in a saturated aqueous solution.

refined Zn–Br_t, Br_t–Zn, Zn–Br_b and Br_b–Zn bond distances of 2.29(2), 2.27(2), 2.388(6) and 2.369(4) Å, respectively; a Zn⋯Zn distance of 2.70(3) Å; and $Br_b\cdots Br_t$ and $Br_b\cdots Br_b$ distances of 3.93(2) and 4.05(4) Å, respectively, Table 4. The results of the EXAFS studies fully support the structure obtained by LAXS. The observed Zn–Br_t and Zn–Br_b bond distances, 2.27 and 2.37 Å, with a mean of 2.34 Å, are significantly shorter than those observed in the $[ZnBr_4]^{2-}$ complexes in the solid state, 2.410 Å (Table S6c). Furthermore, these bond distances are slightly shorter than the mean Zn–Br and Zn–O bond distances in the $[ZnBr_3(H_2O)]^-$ complex in the solid state, which are 2.375 and 2.047 Å, respectively (Table S6a). The most likely structure of the highly concentrated zinc(II) bromide solution is a hydrated dimer, $[Zn_2Br_4(H_2O)_2]$, with Br_t–Zn–Br_b and Br_b–Zn–Br_b bond angles of *ca.* 115°, Fig. 13. This induces a short Zn⋯Zn distance, refined to *ca.* 2.7 Å, Tables 3 and 4. This distance is significantly longer than the Zn–Zn bond distance in dimeric zinc(I) complexes, *ca.* 2.3 Å,[80] and it can be assumed that the ionic radius of zinc(I) is significantly larger than that of zinc(II). If there is any interaction between the zinc atoms, besides the repelling charges between the zinc(II) ions in the $[Zn_2Br_4(H_2O)_2]$ complex, it must be weak. This complex disproportionates to $[Zn(H_2O)_6][Zn_2Br_6]$ at crystallization from aqueous solution.[37]

The RDF of the LAXS data of the highly concentrated aqueous solution of zinc(II) chloride shows two sharp peaks at 2.25 and 3.85 Å, and a broad weak peak at 3.10 Å, Fig. 14, corresponding to Zn–Cl and Cl⋯Cl distances in a dimeric $[Zn_2Cl_4]$ complex with triangular coordination around zinc and to interatomic Cl⋯(H–)O distances in hydrated chloride ions in the $[Zn_2Cl_4]$ complex, respectively. By applying a model with different terminal, Zn–Cl_t, and bridging, Zn–Cl_b, bond distances, these distances were refined to 2.130(5) and 2.225(1) Å, respectively, with a mean of 2.193 Å, and the $Cl_b\cdots Cl_t$, $Cl_b\cdots Cl_b$ and Zn⋯Zn distances to 3.79(1), 3.87(4) and 2.51(2) Å, respectively. The Cl_t–Zn–Cl_b bond angle becomes 121(2)°, showing a triangular coordination of chlorides around zinc, Fig. 13. No water molecules bound to the zinc ions could be detected. It can therefore be assumed that the hydration of the $[Zn_2Cl_4]$ complex takes place through chloride ions. The observed mean Zn–Cl bond distance is shorter than the mean Zn–Cl bond distance in the $[ZnCl_3(H_2O)]^-$ complex in the solid state, 2.242 Å, and significantly shorter than that in the tetrahedral $[ZnCl_4]^{2-}$ complex, 2.270 Å, Tables S6a and S6b (SI). Such a

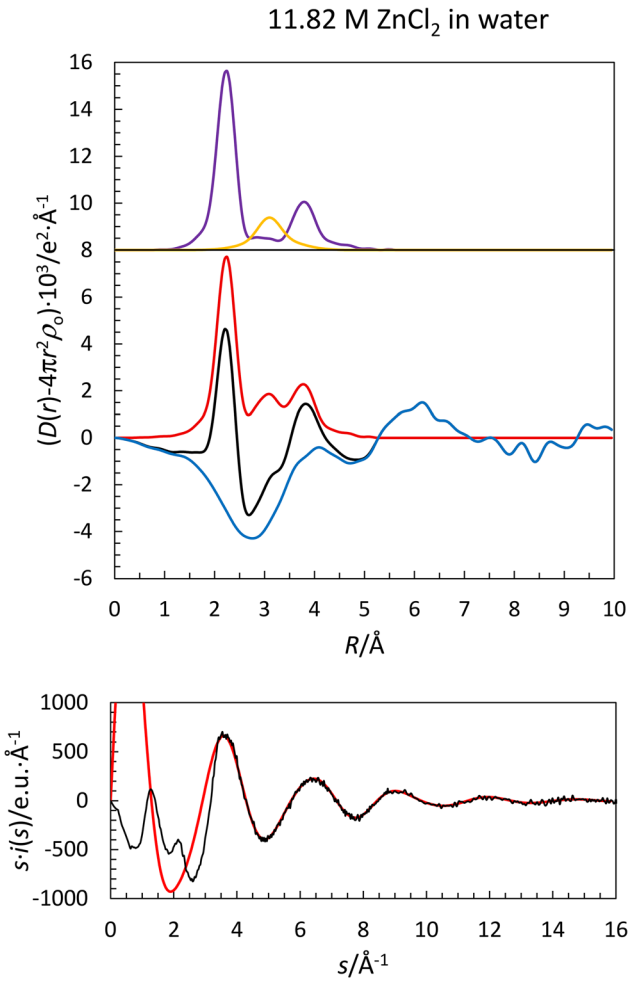

Fig. 14 (Top) LAXS radial distribution curves for an 11.82 mol dm^{-3} aqueous solution of zinc(II) chloride. Upper part: Separate model contributions (offset: 8) of the hydrated tetrachlorodizinc(II) complex (yellow line) and the hydrated chloride ion (cerise line). (Middle) Experimental RDF: $D(r) - 4\pi r^2\rho_0$ (black line); sum of model contributions (red line); difference (blue line). (Bottom) Reduced LAXS intensity functions $s{\cdot}i(s)$ (black line); model $s.i_{calc}(s)$ (red line).

structure induces a short Zn···Zn distance in the complex, *ca.* 2.5 Å.

The aqueous solutions of 1.0 mol dm^{-3} zinc(II) chloride and bromide are expected to contain mixtures of several complexes, Table S1e and Fig. S4 (SI), and thus are difficult to evaluate. It was therefore decided not to perform any studies on such solutions.

Conclusions

The cobalt(II), nickel(II) and copper(II) chloride and bromide systems form no inner-sphere halide complexes in 1.0 mol dm^{-3} aqueous solution, as observed in the EXAFS studies; the EXAFS spectra of these solutions superimpose those of corresponding dilute aqueous perchlorate solutions and the solid perchlorate salts. In a highly concentrated aqueous solution, manganese(II) forms a *cis*-dibromo complex, as also found in the solid state. Cobalt(II) and nickel(II) form one inner-sphere complex with chloride and bromide, and copper(II) with chloride, in highly concentrated aqueous solution. Copper(II) bromide forms a polynuclear complex based on *cis*-$CuBr_2(H_2O)_2$ units connected through a common water molecule in the axial position. This structure is significantly different from the *trans*-$[CuBr_2(H_2O)_2]$ complex formed in the solid state. Zinc bromide forms a hydrated dimeric complex, $[Zn_2Br_4(H_2O)_2]$, with a distorted tetrahedral geometry around zinc in a saturated aqueous solution. Zinc chloride forms a dimeric complex, $[Zn_2Cl_4]$, with a triangular coordination geometry around zinc, and hydration occurs only through the chloride ions in the complex. The structures in the solid state, precipitating from aqueous over-saturated zinc chloride and bromide solutions, $[Zn(H_2O)_6][ZnX_4]$ or $[(H_2O)_5Zn{-}Cl{-}ZnCl_3]$, are significantly different from the structures observed in saturated aqueous solution.

Author contributions

EGB did participate in the LAXS experiments and data treatment and the writing of the manuscript. KGVSC did participate in the EXAFS experiments. IP did participate in the LAXS and EXAFS experiments and is responsible for the final data treatment and evaluation, and the writing of the manuscript.

Conflicts of interest

There are no conflicts of interest to declare.

Data availability

All experimental data are available upon request to author at e-mail: ingmar.persson@slu.se.

Supplementary information: a summary of the stability constants of transition metal-chloride and bromide complexes in dilute aqueous solution, an overview of hydrated transition metal chloride and bromide structures in the solid state, fits of raw EXAFS and Fourier transform data of a 3.59 mol dm^{-3} aqueous solution of copper(II) chloride, and photos of drops of highly concentrated aqueous copper(II) bromide solutions in filter paper. See DOI: **https://doi.org/10.1039/d5dt01840d**.

Acknowledgements

The support from the Swedish Research Council and the Department of Molecular Sciences, SLU, is acknowledged. The MAX IV laboratory, Lund University, is acknowledged for allocation of beam-time during the commissioning period for these studies. Research conducted at MAX IV, a Swedish national user facility, is supported by the Swedish Research council under contract 2018-07152, the Swedish Governmental

Agency for Innovation Systems under contract 2018-04969, and Formas under contract 2019-02496. Dr Lars Eriksson, Department of Materials and Environmental Chemistry, Stockholm University, is acknowledged for plotting Fig. 2, 11 and 13, and the TOC figure.

References

1 https://www.cropnutrition.com/resource-library/manganese-in-crop-production/ (downloaded July 29, 2025).
2 Y. Liu, M. Nan, Z. Zhao, B. Shen, L. Qiao, H. Zhang and X. Ma, Manganese-based flow battery based on the $MnCl_2$ electrolyte for energy storage, *Chem. Eng. J.*, 2023, **465**, 142602, DOI: 10.1016/j.cej.2023.142602.
3 R. Jira, Acetaldehyde from Ethylene—A Retrospective on the Discovery of the Wacker Process, *Angew. Chem., Int. Ed.*, 2009, **48**, 9034–9037, DOI: 10.1002/anie.200903992 and references therein.
4 J. Xiong, S. Yu, H. Zhu, S. Wang, Y. Chen and S. Liu, Dissolution and structure change of bagasse cellulose in zinc chloride solution, *BioResources*, 2016, **11**, 3813–3824, DOI: 10.15376/biores.11.2.3813-3824.
5 S. Sen, B. P. Losey, E. E. Gordon, D. S. Argyropoulos and J. D. Martin, Ionic Liquid Character of Zinc Chloride Hydrates Define Solvent Characteristics that Afford the Solubility of Cellulose, *J. Phys. Chem. B*, 2016, **120**, 1134–1141, DOI: 10.1021/acs.jpcb.5b11400.
6 https://www.oil-drilling-fluids.com (downloaded July 29, 2025).
7 A. Mahmood, Z. Zheng and Y. Chen, Zinc–Bromine Batteries: Challenges, Prospective Solutions, and Future, *Adv. Sci.*, 2023, **11**, 2305561, DOI: 10.1002/advs.202305561.
8 M. H. Bahrin, M. H. A. R. M. Ahmad, H. Hasan, A. A. Rahman, A. Azman, M. Z. Hassan, M. R. B. Mamat, S. S. Muhamad, M. A. Hamzah, R. Jamro, Y. M. Wo and N. Hamssin, Characterization of $ZnBr_2$ solution as a liquid radiation shield for mobile hot cell window, *AIP Conf. Proc.*, 2017, **1799**, 040003, DOI: 10.1063/1.4972927.
9 D. W. Smith, Ionic Hydration Enthalpies, *J. Chem. Educ.*, 1977, **54**, 540–542, DOI: 10.1021/ed054p540.
10 C. E. Housecroft and H. D. Brooke Jenkins, Absolute ion hydration enthalpies and the role of volume within hydration thermodynamics, *RSC Adv.*, 2017, **7**, 27881–27894, DOI: 10.1039/C6RA25804B.
11 I. Persson, Structure and Size of Complete Hydration Shells of Metal Ions and Inorganic Anions in Aqueous Solution, *Dalton Trans.*, 2024, **53**, 15517–15738, DOI: 10.1039/d4dt01449a.
12 J. Stangret and T. Gampe, Ionic Hydration Behaviour Derived From Infrared Spectra in HDO, *J. Phys. Chem. A*, 2002, **106**, 5393–5402, DOI: 10.1021/jp025531j.
13 I. Persson, D. Lundberg, É. G. Bajnoczi, K. Klementiev, J. Just and K. G. V. Sigfridsson Clauss, EXAFS study on the coordination chemistry of the solvated copper(II) ion in a series of oxygen donor solvents, *Inorg. Chem.*, 2020, **59**, 9538–9550, DOI: 10.1021/acs.inorgchem.0c00403.
14 P. Frank, M. Benfatto, M. Qayyam, B. Hedman and K. O. Hogdson, A high-resolution XAS study of aqueous Cu (II) in liquid and frozen solutions: Pyramidal, polymorphic, and non-centrosymmetric, *J. Chem. Phys.*, 2015, **142**, 084310, DOI: 10.1063/1.4908266.
15 Y. Tajiri, M. Ichihashi, T. Mibuchi and H. Wakita, An X-Ray Diffraction Investigation of the Coordination Structure of Mn(II) Ions in Highly Concentrated Aqueous $MnBr_2$ and $MnCl_2$ Solutions, *Bull. Chem. Soc. Jpn.*, 1986, **59**, 1155–1159, DOI: 10.1246/bcsj.59.1155.
16 B. Beagley, C. A. McAuliffe, S. P. B. Smith and E. W. White, EXAFS studies of aqueous solutions of manganese(II) chloride and bromide: structural variations with concentration and interactions with solvent, *J. Phys.: Condens. Matter*, 1991, **3**, 7919–7930, DOI: 10.1088/0953-8984/3/40/013.
17 D. L. Wertz and R. F. Kruh, Solute-Solvent Interactions in Some Concentrated Cobalt(II) Bromide Solutions, *Inorg. Chem.*, 1970, **9**, 595–598, DOI: 10.1021/ic50085a031.
18 D. L. Wertz and R. F. Kruh, X–Ray Diffraction Study of Some Concentrated Cobalt(II) Chloride Solutions, *J. Chem. Phys.*, 1969, **50**, 4313–4317, DOI: 10.1063/1.1670896.
19 M. Magini, Hydration and complex formation study on concentrated MCl_2 solutions [M=Co(II), Ni(II), Cu(II)] by x–ray diffraction technique, *J. Chem. Phys.*, 1981, **74**, 2523–2529, DOI: 10.1063/1.441322.
20 H.-G. Lee, Y. Matsumoto, T. Yamaguchi and H. Ohtaki, X-Ray Diffraction Studies on the Structures of Hydrated Oxonium Ion, and the Chlorocobalt(II) and Tetrachlorocobaltate(II) Complexes in Aqueous Solutions, *Bull. Chem. Soc. Jpn.*, 1983, **56**, 443–448, DOI: 10.1246/bcsj.56.443.
21 G. Paschina, G. Piccaluga, G. Pinna and M. Magini, X-ray investigation of Co-Cl bonding in a concentrated aqueous solution of $CoCl_2$ and LiCl, *Chem. Phys. Lett.*, 1983, **98**, 157–161, DOI: 10.1016/0009-2614(83)87119-X.
22 A. Musinu, G. Paschina, G. Piccaluga and M. Magini, X–ray diffraction study of $CoCl_2$–LiCl aqueous solutions, *J. Chem. Phys.*, 1984, **80**, 2772–2776, DOI: 10.1063/1.447024.
23 M. Ishihashi, H. Wakita and I. Masuda, Structure of iron (II) and cobalt(II) bromide complexes in aqueous solution by X-ray diffraction analysis, *J. Solution Chem.*, 1984, **13**, 505–516, DOI: 10.1007/BF00647175.
24 E. I. Zhilyaeva, G. V. Shilov, D. V. Konarev, A. M. Flakina, R. B. Lyubovskii and R. N. Lyubovskaya, BEDT-TTF based molecular conductor containing the $[Ni(H_2O)_5Br]^+$ magnetic cation, *Synth. Met.*, 2017, **231**, 137–142, DOI: 10.1016/j.synthmet.2017.07.008.
25 H. Ohtaki and T. Radnai, Structure and Dynamics of Hydrated Ions, *Chem. Rev.*, 1993, **93**, 1157–1204, DOI: 10.1021/cr00019a014, and references therein.
26 G. Paschina, G. Piccaluga, G. Pinna and M. Magini, X-ray diffraction and structure of $NiCl_2$ aqueous solutions, *Faraday Discuss. Chem. Soc.*, 1977, **72**, 62–68, DOI: 10.1039/DC9776400062.

27 J. R. Newsome, G. W. Neilson, J. E. Enderby and M. Sandström, Ni^{2+} hydration in perchlorate and chloride solutions, *Chem. Phys. Lett.*, 1981, **82**, 399–401, DOI: 10.1016/0009-2614(81)85406-1.
28 H. Wakita, M. Ichihashi, T. Mibuchi and I. Masuda, The Structure of Nickel(II) Bromide in Highly Concentrated Aqueous Solution by X-Ray Diffraction Analysis, *Bull. Chem. Soc. Jpn.*, 1982, **55**, 817–821, DOI: 10.1246/bcsj.55.817.
29 M. Magini, M. deMoraes, G. Licheri and G. Piccaluga, Composition of the first coordination sphere of Ni^{2+} in concentrated aqueous $NiBr_2$ solutions by x–ray diffraction, *J. Chem. Phys.*, 1985, **83**, 5797–5801, DOI: 10.1063/1.449659.
30 R. Caminiti and P. Cucca, X-ray diffraction study on A $NiBr_2$ aqueous solution. Experimental evidence of the Ni(II)-Br contacts, *Chem. Phys. Lett.*, 1982, **89**, 110–114, DOI: 10.1016/0009-2614(82)83384-8.
31 J. R. Bell, J. L. Tyvoll and D. L. Wertz, Solute structuring in aqueous copper(II) chloride solutions, *J. Am. Chem. Soc.*, 1973, **95**, 1456–1459, DOI: 10.1021/ja00786a018.
32 D. L. Wertz and J. L. Tyvoll, The coordination of Cu(II) in a nearly saturated solution of $CuCl_2$ in hydrochloric acid, *J. Inorg. Nucl. Chem.*, 1974, **36**, 3713–3717, DOI: 10.1016/0022-1902(74)80154-5.
33 M. Magini, Hydration and complex formation study on concentrated MCl_2 solutions [M=Co(II), Ni(II), Cu(II)] by x–ray diffraction technique, *J. Chem. Phys.*, 1981, **74**, 2523–2529, DOI: 10.1063/1.441322.
34 M. Ishihashi, H. Wakita, T. Mubuchi and I. Masuda, Coordination Structure of Cu^{2+} Ion in Highly Concentrated Aqueous $CuBr_2$ Solution, Determined by X-Ray Diffraction Analysis, *Bull. Chem. Soc. Jpn.*, 1982, **55**, 3160–3164, DOI: 10.1246/bcsj.55.3160.
35 R. J. Wilcox, B. P. Losey, J. C. W. Folmer, J. D. Martin, M. Zeller and R. Sommer, Crystalline and liquid structure of zinc chloride trihydrate: a unique ionic liquid, *Inorg. Chem.*, 2015, **54**, 1109–1119, DOI: 10.1021/ic5024532.
36 E. Hennings, H. Schmidt and W. Voigt, Crystal structures of $ZnCl_2{\cdot}2.5\ H_2O$, $ZnCl_2{\cdot}3H_2O$ and $ZnCl_2{\cdot}4.5H_2O$, *Acta Crystallogr., Sect. E:Struct. Rep. Online*, 2014, **70**, 515–518, DOI: 10.1107/S1600536814024738.
37 H. Follner and B. Brehler, Die Kristallstruktur des $ZnCl_2{\cdot}4/3H_2O$, *Acta Crystallogr., Sect. B:Struct. Sci.*, 1970, **26**, 1679–1682, DOI: 10.1107/S0567740870004715.
38 R. Duhlev, I. D. Brown and R. Faggiani, Zinc bromide dihydrate $ZnBr_2{\cdot}2H_2O$: a doublesalt structure, *Acta Crystallogr., Sect. E:Crystallogr. Commun.*, 1988, **44**, 1696–1698, DOI: 10.1107/S0108270188006584.
39 R. F. Kruh and C. L. Standley, An X-Ray Diffraction Study of Aqueous Zinc Chloride Solutions, *Inorg. Chem.*, 1962, **1**, 941–943, DOI: 10.1021/ic50004a050.
40 D. L. Wertz and J. R. Bell, Solute species and equilibria in concentrated zinc chloride/hydrochloric acid solutions, *J. Inorg. Nucl. Chem.*, 1973, **35**, 861–868, DOI: 10.1016/0022-1902(73)80455-5.
41 T. Yamaguchi, S. Hayashi and H. Ohtaki, X-ray diffraction and Raman studies of zinc(II) chloride hydrate melts, $ZnCl_2{\cdot}rH_2O$ (r = 1.8, 2.5, 3.0, 4.0, and 6.2), *J. Phys. Chem.*, 1989, **83**, 2620–2625, DOI: 10.1021/j100343a074.
42 D. L. Wertz, R. M. Lawrence and R. F. Kruh, X–Ray–Diffraction Study of Zinc Bromide Solutions, *J. Chem. Phys.*, 1965, **43**, 2163–2165, DOI: 10.1063/1.1697105.
43 E. Kalman, I. Serke, G. Plálinkás, G. Johansson, G. Kaisch, M. Maeda and H. Ohtaki, Complex Formtion in an Aqueous $ZnBr_2$ Solution Based on Electron Diffraction, X-ray scattering and Raman Spectra, *Z. Naturforsch., A*, 1983, **38**, 225–230, DOI: 10.1515/zna-1983-0220.
44 P. L. Goggin, G. Johansson, M. Maeda and H. Wakita, The structures of zinc bromide complexes in aqueous solution, *Acta Chem. Scand., Ser. A*, 1984, **38**, 625–639, DOI: 10.3891/ACTA.CHEM.SCAND.38A-0625.
45 T. Takamuku, M. Ihara, T. Yamaguchi and H. Wakita, Raman Spectroscopic and X-ray Diffraction Studies on Concentrated Aqueous Zinc(II) Bromide Solution at High Temperatures, *Z. Naturforsch., A:Phys. Sci.*, 1992, **47**, 485–492, DOI: 10.1515/zna-1992-0308.
46 R. Mancinelli, A. Botti, F. Bruni, M. A. Ricci and A. K. Soper, Hydration of Sodium, Potassium, and Chloride Ions in Solution and the Concept of Structure Maker/Breaker, *J. Phys. Chem. B*, 2007, **111**, 13570–13577, DOI: 10.1021/jp075913v.
47 F. Jalilehvand, D. Spångberg, P. Lindqvist-Reis, K. Hermansson, I. Persson and M. Sandström, Hydration of the Calcium Ion. An EXAFS, Large-Angle X-Ray Scattering, and Molecular Dynamics Simulation Study, *J. Am. Chem. Soc.*, 2001, **123**, 431–441, DOI: 10.1021/ja001533a.
48 G. Johansson and M. Sandström, Computer-programs for analysis of data on X-ray-diffraction by liquids, *Chem. Scr.*, 1973, **4**, 195–198.
49 C. M. V. Stålhandske, I. Persson, M. Sandström and E. Kamienska-Piotrowicz, A Large Angle Scattering and Vibrational Spectroscopic Study of the Solvated Zinc, Cadmium and Mercury(II) Ions in *N,N*-Dimethylthioformamide Solution, *Inorg. Chem.*, 1997, **36**, 3174–3182, DOI: 10.1021/ic961339i.
50 *International Tables for X-ray Crystallography*, Kynoch Press, Birmingham, U.K., 1974, vol. 4.
51 D. T. Cromer, Compton Scattering Factors for Aspherical Free Atoms, *J. Chem. Phys.*, 1969, **50**, 4857–4859, DOI: 10.1063/1.1670980.
52 D. T. Cromer and J. B. Mann, Compton Scattering Factors for Spherically Symmetric Free Atoms, *J. Chem. Phys.*, 1967, **47**, 1892–1893, DOI: 10.1063/1.1712213.
53 H. A. Levy, M. D. Danford and A. H. Narten, *Data Collection and Evaluation with an X-ray Diffractometer Designed for the Study of Liquid Structure, Technical Report ORNL-3960*, Oak Ridge National Laboratory, Oak Ridge, TN, 1966. DOI: 10.2172/4524253.
54 M. Molund and I. Persson, STEPLR - A Program for Refinements of Data on X-Ray Scattering by Liquids, *Chem. Scr.*, 1985, **25**, 197–197.
55 K. Klementiev, K. Norén, S. Carlson, K. G. V. Sigfridsson Clauss and I. Persson, The BALDER beam-line at the MAX

IV Laboratory, *J. Phys.:Conf. Ser.*, 2016, **712**, 012023, DOI: 10.1088/1742-6596/712/012023.

56 A. Thompson, D. Attwood, E. Gullikson, M. Howells, K.-J. Kim, K. Kirz, J. Kortright, I. Lindau, Y. Liu, P. Pianetta, A. Robinson, J. Scofield, J. Underwood, G. Williams and H. Winick, in *X-ray Data Booklet*, Lawrence Berkley National Laboratory, 2009; available at https://xdb.lbl.gov/xdb.pdf (downloaded July 29, 2025).

57 G. N. George and I. J. Pickering, in *EXAFSPAK - A Suite of Computer Programs for Analysis of X-ray Absorption Spectra*, SSRL, Stanford, CA, 1993; available at https://www-ssrl.slac.stanford.edu/exafspak.html (downloaded July 29, 2015).

58 S. I. Zabinsky, J. J. Rehr, A. Ankudinov, R. C. Albers and M. J. Eller, Multiple-Scattering Calculations of X-ray Absorption Spectra, *Phys. Rev. B: Condens. Matter Mater. Phys.*, 1995, **52**, 2995–3009, DOI: 10.1103/PhysRevB.52.2995.

59 K. Sudarsanan, Manganese bromide tetrahydrate, *Acta Crystallogr., Sect. B*, 1975, **31**, 2720–2721, DOI: 10.1107/S056774087500862X.

60 J.-H. P. Lee, B. D. Lewis, J. M. Mendes, M. M. Turnbull and F. F. Awwadi, Transition metal halide salts and complexes of 2-aminopyrimidine: manganese(II) compounds – crystal structures of (2-aminopyrimidinium)$_4$[MnCl$_4$(H$_2$O)]$_2$, [(2-aminopyrimidine)$_2$MnBr$_2$(H$_2$O)$_2$ ·2H$_2$O and (2-aminopyrimidinium)$^{2+}$ [MnBr$_2$(H$_2$O)$_4$]Br$_2$, *J. Coord. Chem.*, 2003, **56**, 1425–1442, DOI: 10.1080/0095897031000164259 1.

61 A. N. Chekhlov, Synthesis and crystal structure of octaaqua (di-μ-bromo)dimanganese(II) dibromide 18-crown-6, *Russ. J. Inorg. Chem.*, 2006, **51**, 1908–1912, DOI: 10.1134/S0036023606120114.

62 V. Falkowski, A. Zeugner, A. Isaeva, K. Wurst, M. Ruck and H. Huppertz, Synthesis and characterization of the manganese hydroxide halides Mn(OH)X (X = Br, I) and crystal structure of *trans*–MnBr$_2$·4H$_2$O, *Z. Anorg. Allg. Chem.*, 2019, **645**, 919–926, DOI: 10.1002/zaac.201900103.

63 H. Bouteiller, M. Pasturel and P. Lemoine, On the crystal structures of the polymorphs of manganese(II) chloride tetrahydrate: *α*-MnCl$_2$·4H$_2$O and *β*-MnCl$_2$·4H$_2$O, *J. Chem. Crystallogr.*, 2021, **51**, 311–316.

64 I. Persson, M. Sandström, H. Yokoyama and M. Chaudhry, Structures of the Solvated Barium and Strontium Ions in Aqueous, Dimethyl Sulfoxide and Pyridine Solution, and Crystal Structure of Strontium and Barium Hydroxide Octahydrate, *Z. Naturforsch., A:Phys. Sci.*, 1995, **50**, 21–37, DOI: 10.1515/zna-1995-0105.

65 Z. Duan, Y. Zhang, B. Zhang and D. Zhu, Solvent-mediated crystal-to-crystal transformation within the CoBr$_2$(1,4-dioxane)$_m$,(H$_2$O)$_n$ family (*m* = 2, 3; *n* = 0, 2, 4) from 2D to 1D, and 0D, *CrystEngComm*, 2011, **13**, 6801–6810, DOI: 10.1039/C1CE05668A.

66 A. C. Blackburn, J. R. Gallucci and R. E. Gerkin, R.E. Structure of tetraaquacobalt(II) bromide dihydrate (cobalt bromide hexahydrate), *Acta Crystallogr., Sect. C:Cryst. Struct. Commun.*, 1991, **47**, 282–286, DOI: 10.1107/S0108270190008083.

67 K. Waizumi, H. Masuda and H. Ohtaki, X-ray structural studies of FeBr$_2$·4H$_2$O, CoBr$_2$·4H$_2$O, NiCl$_2$·4H$_2$O and CuBr$_2$·4H$_2$O. *Cis*/*trans* selectivity in transition metal(II) dihalide tetrahydrate, *Inorg. Chim. Acta*, 1992, **192**, 173–181, DOI: 10.1016/S0020-1693(00)80756-2.

68 M. Ichihashi, H. Wakita and I. Masuda, Structure of Iron (II) and Cobalt(II) Bromide Complexes in Aqueous Solution by X-ray Diffraction Analysis, *J. Solution Chem.*, 1984, **13**, 505–516, DOI: 10.1007/BF00647175.

69 M. Louer, D. Grandjean and D. Weigel, Structure cristalline et expansion thermique de l'iodure de nickel hexahydrate, *J. Solid State Chem.*, 1973, **7**, 222–228, DOI: 10.1016/0022-4596(73)90157-6.

70 A. N. Chekhlov, *trans*-Tetraaqua(dibromo)nickel(II) 4,7,13,16,21,24-hexaoxa-1,10-diazoniabicyclo[8.8.8]hexacosane dibromide: Synthesis and crystal structure, *Russ. J. Coord. Chem.*, 2007, **33**, 335–345, DOI: 10.1134/S1070328407050041.

71 J. C. Barnes and T. J. R. Weakley, Role of 1,4-dioxan in solid adducts of hydrated metal halides. Crystal structures of hexaaquadichloromagnesium-1,4-dioxan(1/1), *trans*-tetraaquadibromonickel(II)–1,4-dioxan(1/2), and *cis*-diaquatetrabromotin(IV)–1,4-dioxan(1/2, *J. Chem. Soc., Dalton Trans.*, 1976, 1786–1790, DOI: 10.1039/DT9760001786.

72 J. W. Steed, B. J. McCool and P. C. Junk, Hydrogen bonded polymers and oligomers from metal salts and 18-crown-6, *J. Chem. Soc., Dalton Trans.*, 1998, 3417–3423, DOI: 10.1039/A805492D.

73 M. E. Masaki, B. J. Prince and M. M. Turnbull, Transition Metal Halide Salts and Complexes of 2-Aminopyrimidine: Cobalt(II) and Nickel(II) compounds, Crystal Structures of Bis(2-Aminopyrimidinium)MX$_4$ [M = Co, Ni; X = Cl, Br] and 2-Aminopyrimidinium(+2) [NiBr$_2$(H$_2$O)$_4$]Br$_2$, *J. Coord. Chem.*, 2002, **55**, 1337–1351, DOI: 10.1080/0095897021000036587.

74 H. Wakita, M. Lchihashi, T. Mibuchi and I. Masuda, The Structure of Nickel(II) Bromide in Highly Concentrated Aqueous Solution by X-Ray Diffraction Analysis, *Bull. Chem. Soc. Jpn.*, 1982, **55**, 817–821, DOI: 10.1246/bcsj.55.817.

75 B. Wang, Diaquadibromidocopper(II)–18-crown-6–water (1/1/2), *Acta Crystallogr., Sect. E:Struct. Rep. Online*, 2010, **66**, m836–m836, DOI: 10.1107/S1600536810023500.

76 E. Arte, J. Feneau-Dupont, J. P. Declercq, G. Germain and M. van Meerssche, Complexe 1 : 1 pentaoxa-1,4,7,10,13 cyclopentadécanebromure de cuivre(II) hydraté, *Acta Crystallogr., Sect. B:Struct. Sci.*, 1979, **35**, 1215–1217, DOI: 10.1107/S056774087900594X.

77 J. Shi, Y. Zhang, B. Zhang and D. Zhu, Crystal-to-crystal transformation from a chain compound to a layered coordination polymer, *Dalton Trans.*, 2016, **45**, 89–92, DOI: 10.1039/C5DT03985A.

78 J. A. Schlueter, H. Park, G. J. Halder, W. R. Armand, C. Dunmars, K. W. Chapman, J. L. Manson, J. Singleton, R. McDonald, A. Plonczak, J. Kang, C. Lee, M.-H. Whangbo, T. Lancaster, A. J. Steele, I. Franke, J. D. Wright, S. Blundell, F. L. Pratt, J. deGeorge, M. M. Turnbull and P. Landee, Importance of

Halogen···Halogen Contacts for the Structural and Magnetic Properties of CuX_2(pyrazine-*N*,*N*′-dioxide)$(H_2O)_2$ (X = Cl and Br), *Inorg. Chem.*, 2012, **51**, 2121–2129, DOI: 10.1021/ic201924q.

79 C. Yue, Z. Lin, L. Chen, F. Jiang and M. Hong, The 2D–3D networks with infinite channels or difform chains of copper(II) complexes via weak non-covalent interactions, *J. Mol. Struct.*, 2005, **779**, 16–22, DOI: 10.1016/j.molstruc.2005.07.013.

80 R. H. Duncan Lyngdoh, H. F. Schaefer III and R. B. King, Metal-Metal (MM) Bond Distacnes and Bond Orders in Binuclear Metal Complexes of the First Row Transition Metals Titanium Through Zinc, *Chem. Rev.*, 2018, **118**, 11626–11706, DOI: 10.1021/acs.chemrev.8b00297.